Clearly, rat Mrp2 accepts many organic anions as substrates. However, its broad substrate specificity has not been investigated in terms of the three-dimensional (3D) structures of ligands (17), and the complete 3D structure has not been determined for any mammalian transporter. Elucidating the structural characteristics of the ligand-binding region of rat Mrp2 would be useful for understanding its broad substrate specificity. Therefore, in the current study, we investigated the binding conformation of ligands to rat Mrp2, the key functional groups for binding to Mrp2 (3D pharmacophore), and the 3D quantitative structure-activity relationships (3D-QSAR) between ligands and rat Mrp2. Our combined method comprised the following three procedures: first, conformational analysis (CAMDAS) (18); second, a molecular superposition procedure (SUPERPOSE) (19); and third, 3D-QSAR analysis by comparative molecular-field analysis (CoMFA) (20). These techniques are described in more detail in the following section.

MATERIALS AND METHODS

Conformational Analysis: Sampling of a Set of Conformers of a Molecule

X-ray structural analysis of protein-ligand complexes has revealed that the binding conformation is one of the stable conformations of a ligand molecule. To generate a set of conformers of ligands, we used the automated program Conformational Analyzer with Molecular Dynamics and Sampling (CAMDAS), which was developed by Tsujishita and Hirono (18). CAMDAS performs high-temperature molecular dynamics (MD) calculations for a target molecule and for sampled conformers that appear during the MD. It then evaluates the similarities between each of the sampled conformers in terms of dihedral angle values, clusters similar conformers together, and, finally, prints out the clustered conformers. In this way, CAMDAS can find the representative conformers from an arbitrarily given structure of the molecule.

To estimate the binding conformation of ligands to rat Mrp2, MD dynamics calculations were executed for 18 ligands (a training set for constructing QSAR models comprising compounds **1–16** and a test set for verifying the QSAR models comprising compounds **A** and **B**), and many conformers were sampled; their chemical structures are shown in Figs. 1 and 2. An MD calculation for sampling was performed for 800 ps with an integral time step of 0.001 ps using an MM2 force field (21) without electrostatic and hydrogen-bonding interactions. The temperature of the system was maintained at 1200 K, and the length of the covalent bonds was fixed using the SHAKE algorithm throughout the MD simulations. Conformers were sampled at every 100 steps and preclustered with dihedral angles during the MD simulations. If the difference between conformers was within ±30°, they were grouped together. Subsequently, reclustering of the sampled conform-

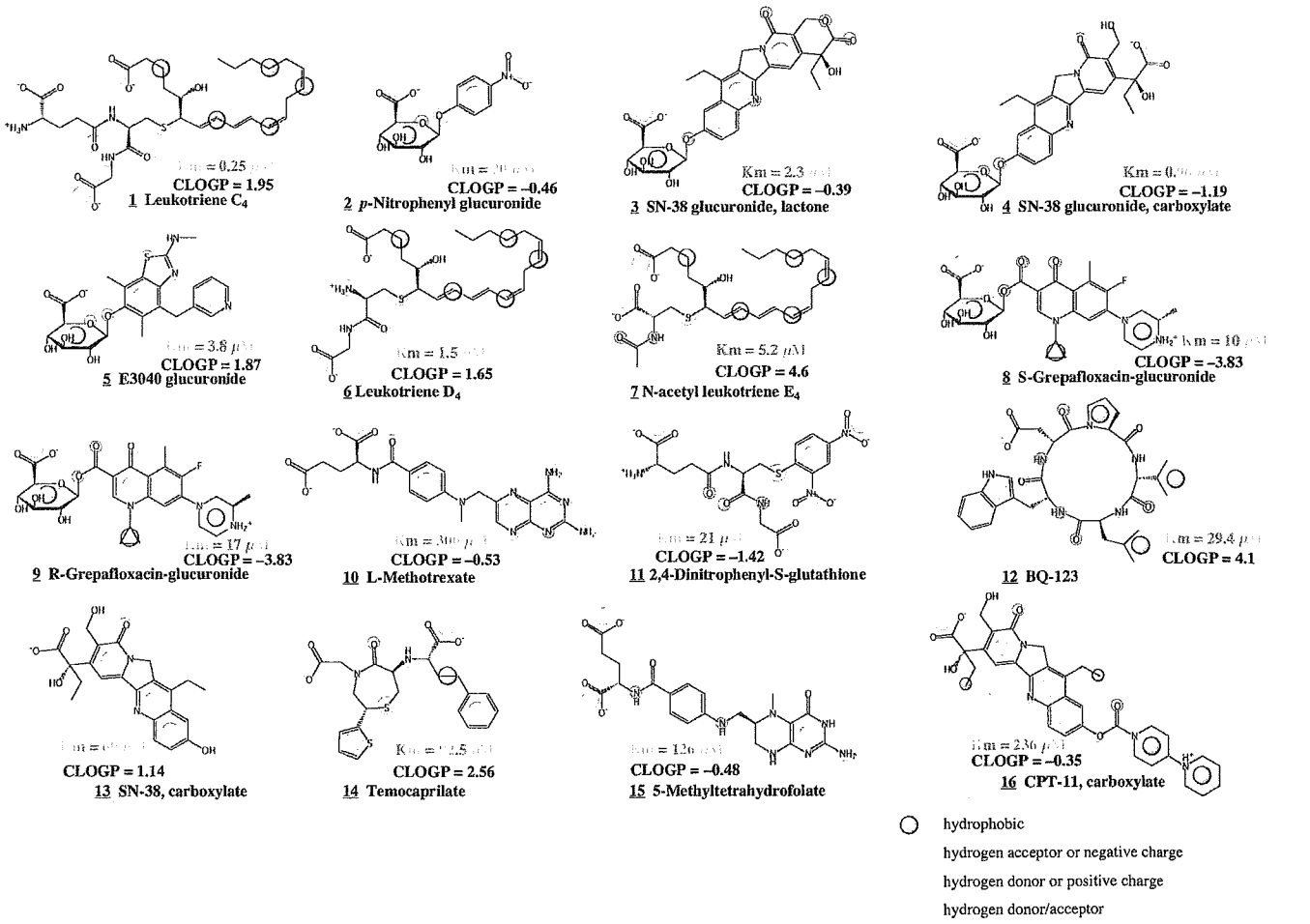

Fig. 1. Chemical structures of the compounds in the training set, with property spheres, K_m, and C log P values.

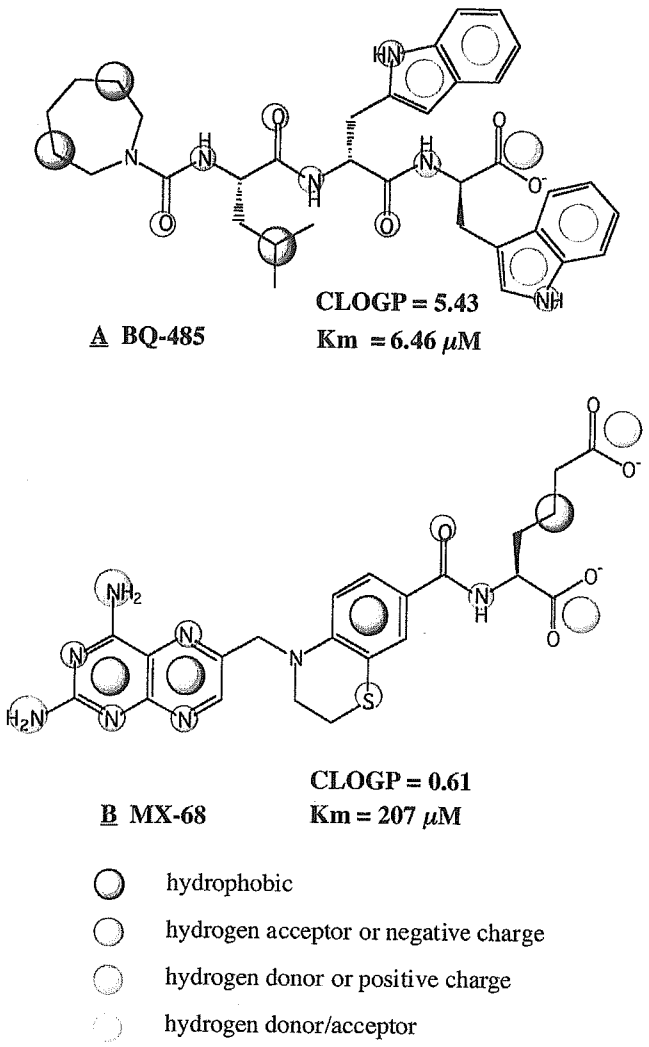

Fig. 2. Chemical structures of the compounds in the test set, with property spheres, K_m, and C log P values.

ers was performed with dihedral angles within ±30°. Before the clustering, each conformer was minimized until the root-mean-square (rms) of the gradients of the potential energy was below 0.004 kcal mol^{-1} $Å^{-1}$.

Molecular Superposition: Selection of the Candidate Binding Conformations

X-ray crystallographic studies of protein-ligand complexes have demonstrated that when ligands bind to a given protein, such as a receptor or a transporter, the atomic groups in the ligands that interact with amino-acid residues of the protein occupy the same 3D space. Based on this information, we carried out molecular superposition for ligand molecules using the SUPERPOSE program developed by Iwase and Hirono (19). The program superposes two molecules based on the physicochemical properties of the atomic groups, which is useful for elucidating a pharmacophore and estimating a binding conformation by distinguishing it from among the many conformations that are generated by high-temperature MD calculations.

Five types of physicochemical properties are considered in the program, including hydrophobic (aromatic), hydrogen-bond donors, hydrogen-bond acceptors, and hydrogen-bond donors/acceptor. Each type is represented as a sphere with a predefined radius and is assigned to a functional group in a molecule. After molecular superposition, the overlaps of the spheres are scored.

The program works as follows. First, a large molecule with its physicochemical properties represented by spheres is fixed at the center of a large box, and another smaller molecule, also with spheres representing its physicochemical properties, is translated and rotated in the box. The translational increment is 1 Å, and the center of mass is translated onto the body-centered-cubic lattice-points made in the circumscribed large-volume rectangular box. The rotation is performed on each of the lattice points. The ranges of the three Eulerian angles are $0° \leq \phi, \varphi < 360°$, and $0° \leq \theta \leq 180°$. The rotational increment is 4°. Second, at every translation or rotation, the property spheres that overlap are determined by calculating the distances between the spheres of the molecules. Third, overlaps of the spheres are scored so that points are added when atomic groups with the same physicochemical properties overlap, and points are subtracted when atomic groups with different physicochemical properties overlap, according to the scoring table (19). Atomic groups without overlaps are not scored.

These three operations are repeated to determine the orientation with the highest score and the smallest rms deviation (rmsd) of the distances of the overlapped atomic groups between the two molecules.

3D-QSAR Analyses: Determination of the Binding Conformation Using CoMFA

The SUPERPOSE program identified several plausible binding conformations. We therefore carried out comparative molecular field analysis (CoMFA) to determine the binding conformation of ligands to rat Mrp2 and to obtain 3D structure-activity relationships.

Table I. Results of Conformational Analysis by CAMDAS

	Number of conformers	ΔE (kcal/mol)	Number of conformers within 12 kcal/mol
Training set			
1	7777	15.570	3846
2	16	14.406	15
3	262	18.565	234
4	876	18.877	798
5	251	16.972	240
6	7777	13.951	5723
7	3121	1112.579	1576
8	479	54.432	316
9	264	32.593	180
10	2547	1013.488	2387
11	3957	978.039	3530
12	5937	53.872	1533
13	177	13.669	176
14	3078	52.334	2832
15	3069	1028.764	2915
16	5135	32.084	3856
Test set			
A	36	480.492	20
B	7777	86.823	4966

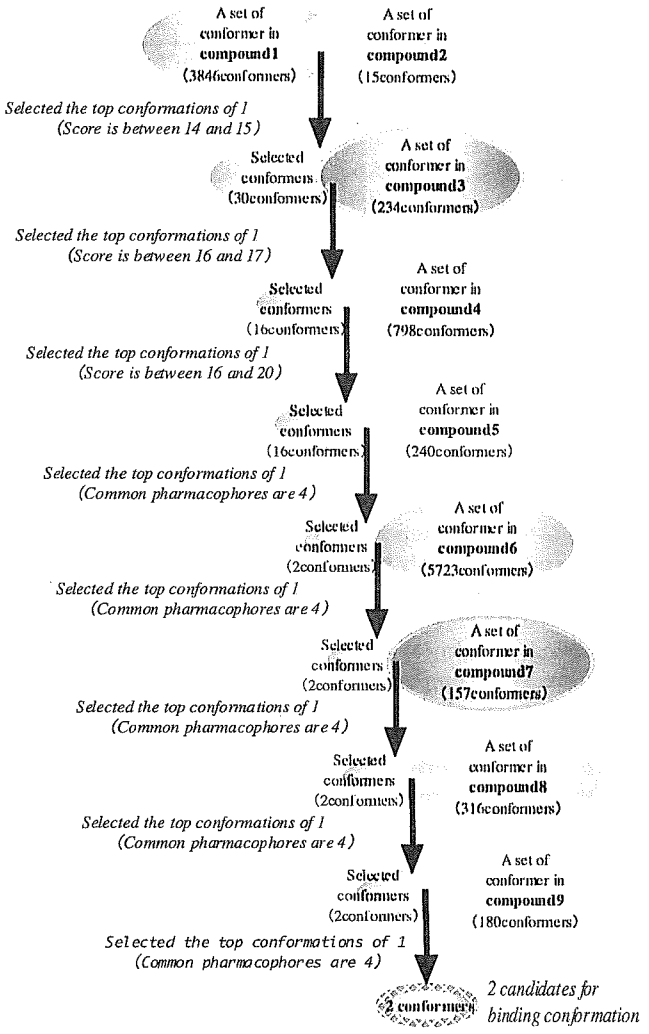

Fig. 3. Flowchart of SUPERPOSE.

The atomic charges of each conformer were calculated using the semiempirical molecular orbital program package MOPAC93 MNDO/ESP, in order to evaluate the electrostatic field in CoMFA. Conventional CoMFA was performed using the QSAR option of SYBYL (Tripos, Inc., St. Louis, MO, USA), with the Michaelis constant (K_m) (22) of each ligand included as bioactive data, as shown in Figs. 1 (training set) and 2 (test set). For the K_m-determination experiments, CMVs were prepared from male Sprague-Dawley (SD) rats, and the transport study was performed using the rapid-filtration technique, as described previously (11,12). All of the compounds were mainly excreted into the bile via rat Mrp2, as biliary excretion in EHBRs and/or the ATP-dependent uptake of each compound into CMVs prepared from EHBRs was disrupted. Therefore, the K_m values for the uptake into CMVs prepared from SD rats corresponded to those for rat Mrp2.

Two calculations were carried out, using an sp^3 carbon probe atom with a charge of +1 and either the steric and electrostatic components or the steric, electrostatic, and calculated log P (C log P) components. The calculated values of log P were estimated using the CLOGP program (Daylight, C.I.S. Inc., Rochester, NY, USA). The CoMFA QSAR equations were calculated with the partial least squares (PLS) algorithm. The optimal number of components in the final CoMFA PLS model was determined using the cross-validated R^2 (q^2) values obtained from the leave-one-out cross-validation technique. The CoMFA PLS model with the highest q^2 values was selected to estimate the binding conformation of ligands for rat Mrp2.

RESULTS

Sampling of a Set of Conformers of Each Ligand

Using the CAMDAS program, we carried out conformational analyses of ligand molecules bound to rat Mrp2. The high-temperature MD calculation was used with a potential function without an electrostatic interaction term and a hydrogen-bonding term to avoid undesirable intramolecular interactions (Figs. 1 and 2). The CAMDAS calculations gave many conformers of the 18 compounds, as shown in Table I. The sets of conformers of compounds **1–9**, the structures of which were significantly different from one another and showed relatively low K_m values, were used by the SUPERPOSE

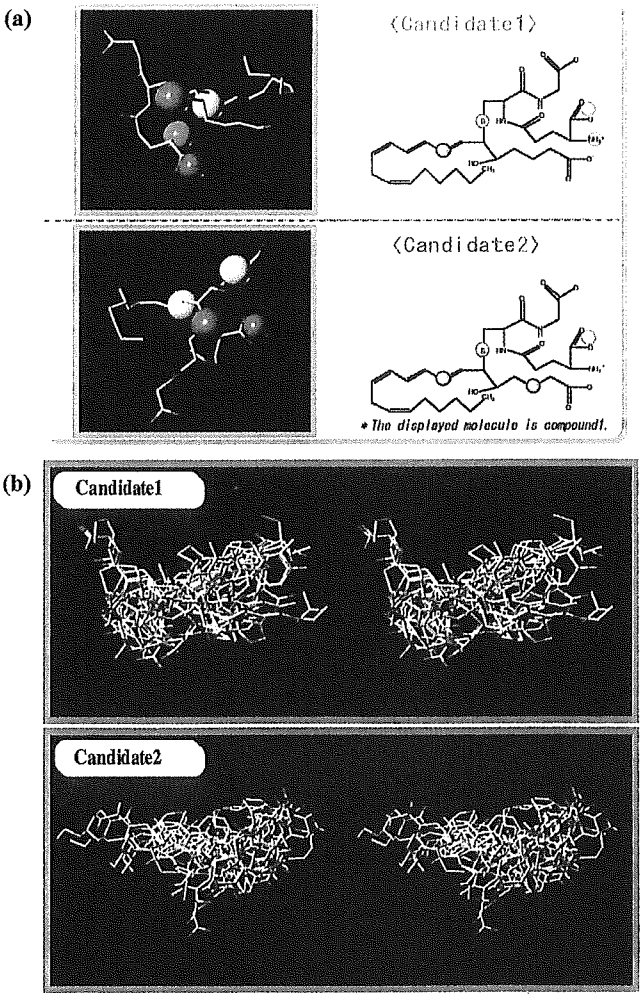

Fig. 4. (a) Property spheres common to compounds **1–9**. (b) Stereo views of superposed compounds in the training set (yellow molecule: compound **1**).

Table II. Results of CoMFA

Field type		Candidate 1		Candidate 2	
		ST + EL	ST + EL + C log P	ST + EL	ST + EL + C log P
Cross-validated	q^2	0.03	0.01	0.36	0.59
	s_{press}	1.21	1.15	0.80	0.64
No. of components		7	6	3	3
Conventional	r^2	1.00	1.00	0.99	0.99
	F	30122.14	2114.33	485.66	613.30
	s	0.01	0.03	0.09	0.08
Contribution (%)	ST	56.6	53.1	60.2	63.0
	EL	43.4	40.5	39.8	33.4
	C log P[a]	—	6.4	—	3.6

St, steric field; EL, electrostatic field; CoMFA, comparative molecular-field analysis.
[a] log P calculated by CLOGP.

program to determine the 3D pharmacophore of the ligand and to obtain the candidate binding conformations.

Selection of Candidate Binding Conformations

As shown in Table I, relatively stable conformers with molecular energies within 12 kcal/mol from the global minimum were selected as the conformers to be superposed. The cutoff value of 12 kcal/mol was confirmed in our previous study (19). For each ligand, the atomic groups that the property spheres were assigned to are shown in Figs. 1 (training set) and 2 (test set).

Initially, 3846 conformers of compound **1** and 15 conformers of compound **2** were superposed (Fig. 3). Each overlap was ranked on the basis of the SUPERPOSE score and the rmsd. As a result, we selected 30 conformers of compound **1** that represented good overlaps, with scores ranging between 14 and 15. Next, these 30 conformers of compound **1** and 234 conformers of compound **3** were superposed. As a result, we selected 16 conformers of compound **1** that showed good overlaps with conformers of compound **3**, with scores ranging between 16 and 17. The 16 selected conformers of compound **1** were then superposed to 798 conformers of compound **4**. No change was observed in the number of good overlaps at this stage, with scores ranging between 16 and 20 for all of the conformers. All 16 conformers of compound **1** were therefore superposed with 240 conformers of compound **5**. There were only two good overlaps for the superposition of compound **1** with compound **5**, with four commonly overlapped functional groups. Using the same method, the selected conformers of compound **1** were superposed to conformers of compounds **6–9** (Fig. 3). We finally obtained two conformers of compound **1** that were considered to be good candidates for the binding conformation. Figure 4a shows the common property spheres; namely, the pharmacophores obtained by superposition using compounds **1–9**.

Next, each candidate for the binding conformation was superposed to conformers of compounds **10–16** in the training set. The atomic groups that the ligand property spheres were assigned to are shown in Fig. 1. In this way, candidate binding conformations of compounds **10–16** were obtained. We then estimated the molecular alignment of ligand molecules (compounds **1–16**) that were essential to CoMFA (Fig. 4b). The

Table III. The Values of $\log(1/K_m)$ Calculated Using the Final CoMFA QSAR Model Compared with Experimental Data

	Experimental	Calculated	Residual
Compounds in the training set			
1 Leukotriene C4	6.60	6.70	−0.10
2 *p*-Nitrophenyl glucuronide	4.70	4.60	0.10
3 SN-38 glucuronide, lactone	5.64	5.63	0.01
4 SN-38 glucuronide, carboxylate	6.02	5.90	0.12
5 E3040 glucuronide	5.42	5.36	0.06
6 Leukotriene D4	5.82	5.77	0.05
7 *N*-acetyl leukotriene E4	5.28	5.33	−0.05
8 (*S*)-Grepafloxacin-glucuronide	5.00	5.00	0.00
9 (*R*)-Grepafloxacin-glucuronide	4.77	4.83	−0.06
10 L-Methotrexate	3.52	3.47	0.05
11 2,4-Dinitrophenyl-*S*-glutathione	4.68	4.76	−0.08
12 BQ-123	4.53	4.46	0.07
13 SN-38, carboxylate	4.16	4.25	−0.09
14 Temocaprilate	4.03	4.09	−0.06
15 5-Methyltetrahydrofolate	3.90	3.84	0.06
16 CPT-11, carboxylate	3.63	3.69	−0.06
Compounds in the test set			
A BQ-485	5.19	5.10	0.09
B MX-68	3.68	4.16	−0.48

two candidates of binding conformation of ligands for rat Mrp2 generated two types of molecular alignments, as shown in Fig. 4b. We also obtained binding conformation candidates for compounds **A–B** for the test set using a similar method to the training set. The test set was used to evaluate the predictive power of the CoMFA model obtained using the training set.

Determination of the Binding Conformation by CoMFA

CoMFA calculations were carried out using the two molecular alignments. The atomic charges of each conformer were calculated using MOPAC93 MNDO/ESP to evaluate the electrostatic field in CoMFA. Conventional CoMFA was performed with the QSAR option of SYBYL. For each molecular alignment (candidate 1 and candidate 2), two types of calculations were carried out together with an sp^3 carbon probe atom with a +1 charge: the first used steric and electrostatic fields, and the second used steric and electrostatic fields along with calculated values of log P (C log P). The CoMFA QSAR equations were calculated with the PLS algorithm. The optimal number of components in the final CoMFA PLS model was determined using the cross-validated R^2 (q^2) values obtained by the leave-one-out technique. The cross-validated R^2 (q^2) values, the standard error of the predictive sum of squares (s_{press}), and the standard error of the estimate (r^2) are listed in Table II for each candidate. The CoMFA PLS model with the highest q^2 values was assumed to best explain the binding conformation.

A good CoMFA model with three PLS components was obtained using the steric and electrostatic fields along with C log P for candidate 2. The final CoMFA model had a q^2 value of 0.59 with six PLS components, an s_{press} value of 0.64, an r^2 value of 0.99, and a standard error of 0.08. The experimental and calculated values of $\log(1/K_m)$ for each compound in the training set are listed in Table III. The property spheres shown in Fig. 5 illustrate the important atomic groups for the binding of each ligand molecule to rat Mrp2.

We also investigated the predictivity of the final CoMFA model using the test set of compounds. The values of $\log(1/K_m)$ calculated using the CoMFA model of candidate 2 with the steric field, electrostatic field, and C log P showed good agreement with the experimental values (Table III). We therefore concluded that the 3D structure of candidate 2 reflects the binding conformation of ligands for rat Mrp2. In the test set, the calculated value of $\log(1/K_m)$ for BQ-485 (5.10) compared well with the experimental value (5.19), whereas the calculated value of MX-68 contained a larger error (0.48). This might be the result of the difficulties of determining the atomic charges of MX-68, which has a pteridine ring, using MOPAC93 MNDO/ESP.

Figure 6a shows a contour map of the steric field from the final CoMFA model, together with the binding conformation of compound **1**: the green contours indicate areas in which bulky atomic groups are sterically favorable for the binding affinity, and the yellow contours indicate areas in which bulky groups are unfavorable for the binding affinity. Figure 6b shows a contour

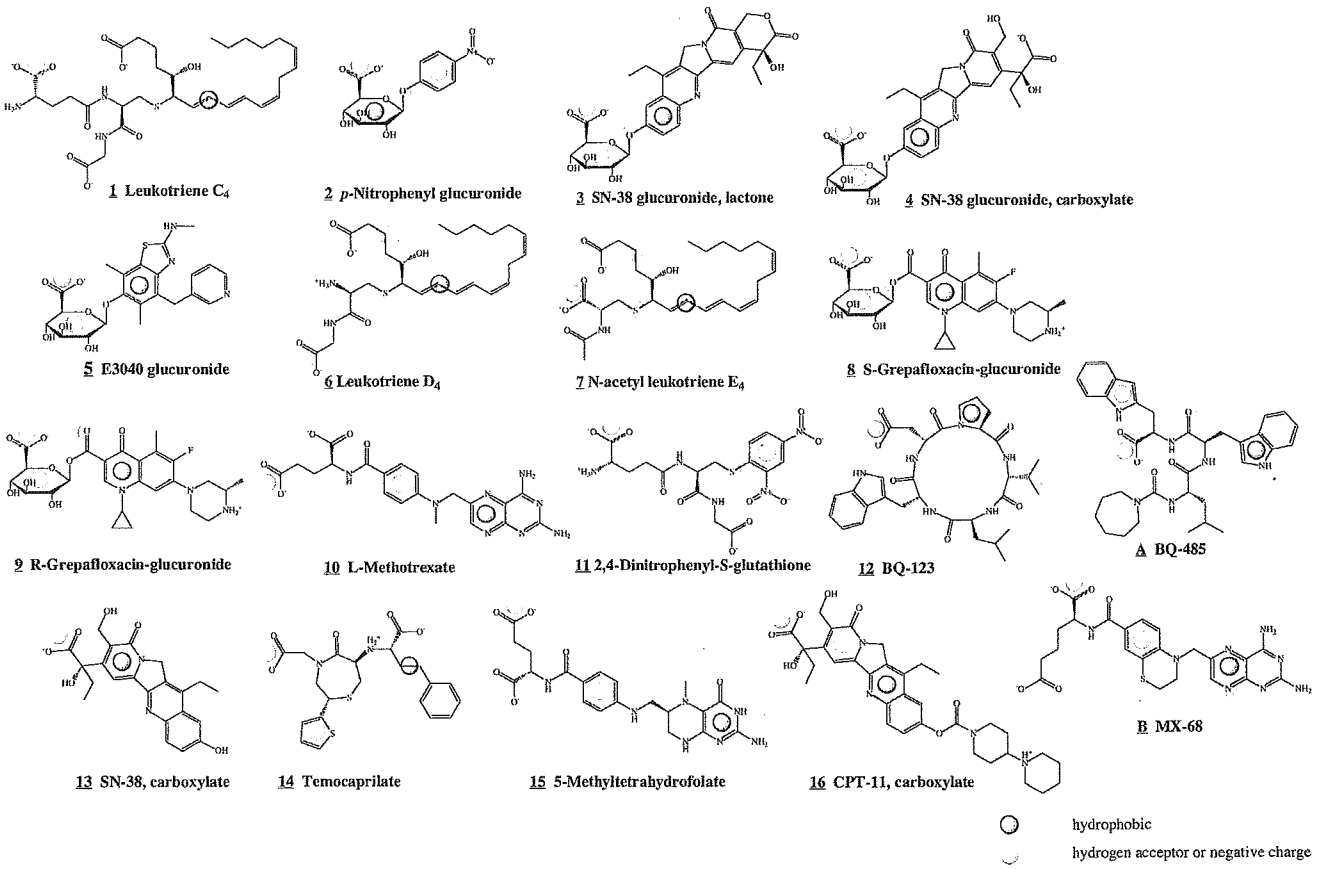

Fig. 5. Atomic groups involved in the binding of each ligand molecule to Mrp2/ABCC2.

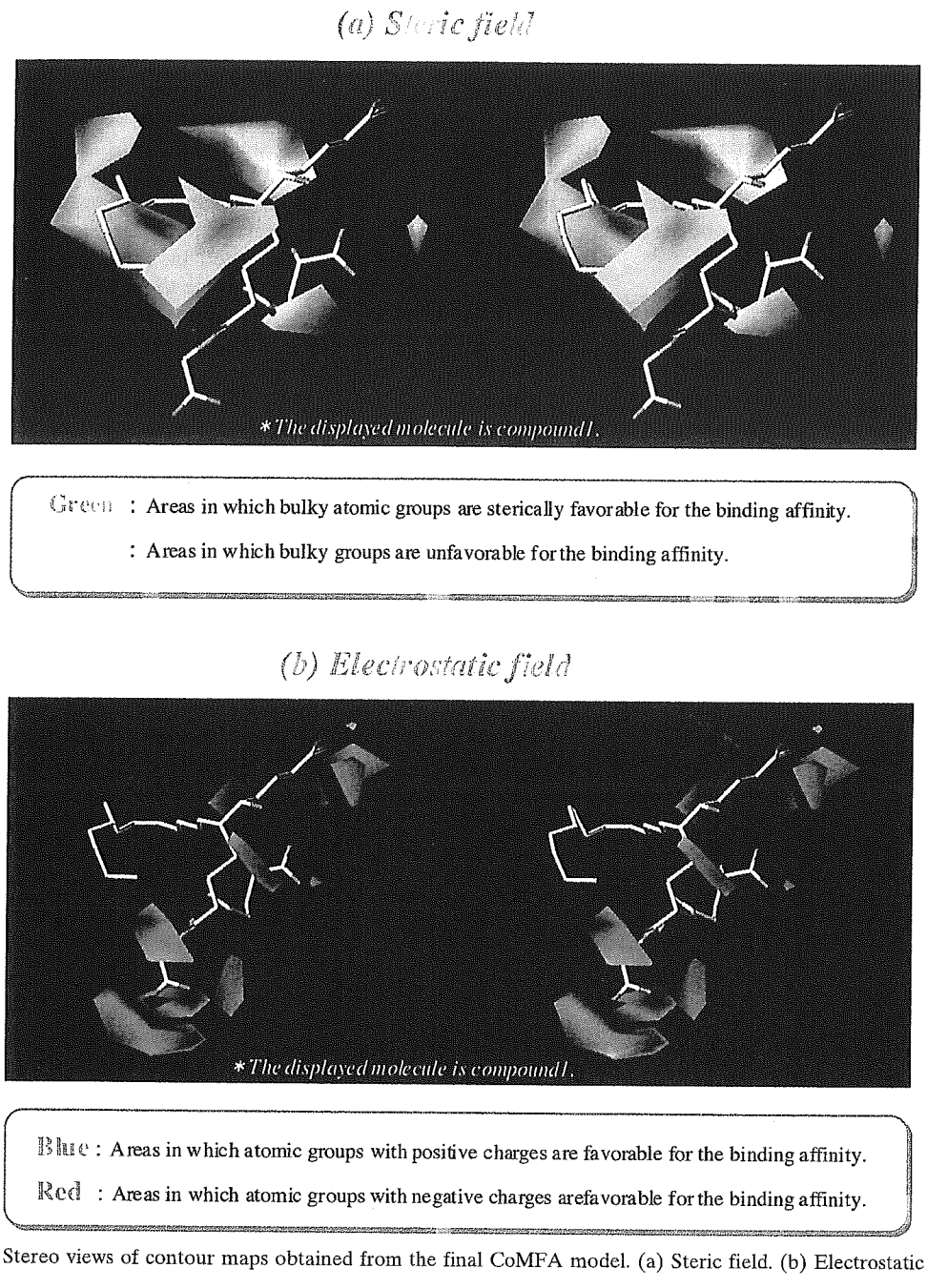

Fig. 6. Stereo views of contour maps obtained from the final CoMFA model. (a) Steric field. (b) Electrostatic field.

map of the electrostatic field from the final CoMFA model, together with the binding conformation of compound **1**: the blue contours indicate areas in which atomic groups with positive charges are advantageous to the binding of ligand with rat Mrp2, and the red contours show areas in which atomic groups with negative charges are favorable for the binding of ligand with rat Mrp2. The areas shown in the contour map are of great importance for explaining variation in the binding affinities of ligands with rat Mrp2.

DISCUSSION

Pharmacophore of Ligands for Rat Mrp2

We have identified a plausible binding conformation of ligands to rat Mrp2 by making full use of ligand-based drug design techniques. In this conformation, four property spheres that are common to all ligands were identified using the SUPERPOSE calculation. We propose that the spatial arrangement of the four functional groups expressed by these property spheres represents a 3D pharmacophore of ligands for rat Mrp2. Figure 7 shows a stereo view of these four property spheres along with the 3D structure of compound **1** and its structural formula. It appears that two hydrogen bond–acceptor groups (HA1 and HA2) and two hydrophobic groups (HP1 and HP2) are essential for the binding of ligands to rat Mrp2 and that these groups constitute the 3D pharmacophore. Figure 8 shows the relative distances between the four property spheres that represent the essential functional groups for ligand binding. The distances are as follows: HA1–HA2, ~5.0 &ARING;; HA1–HP1, ~5.3 &ARING;; HA1–

HP2, ~5.5 &ARING;; HA2–HP1, 4.7 &ARING;; HA2–HP2, 3.2 &ARING;; and HP1–HP2, 4.8 &ARING;.

Estimation of the Ligand-Binding Site of Rat Mrp2

A good CoMFA model was identified with the following parameters: a q^2 value of 0.59 with six PLS components, an s_{press} value of 0.64, an r^2 value of 0.99, and a standard error of 0.08. We suggest that the success of the CoMFA was a result of the use of the molecular alignment obtained using SUPERPOSE. This represents a unique and distinctive approach, in which the binding conformation and 3D pharmacophore of a ligand are estimated using ligand-based drug design techniques and are then applied to the molecular alignment, which is essential to CoMFA.

On the basis of the 3D pharmacophore and the contour map obtained from the CoMFA calculation, we have estimated the structure of the ligand-binding site of rat Mrp2 (Fig. 9). The four primary binding sites correspond to the 3D pharmacophore, comprising the four functional groups that are essential for the binding of ligands to rat Mrp2. The model also suggests that secondary binding sites, which correspond to specific contour levels in the CoMFA contour map, are important in explaining the variation of the binding affinities of ligands to rat Mrp2.

In conclusion, we propose that both hydrophobic and electrostatic interactions have vital roles in the binding of ligands to rat Mrp2. Ligand recognition seems to be achieved through interactions in the two hydrophobic sites and the two electrostatically positive sites (primary binding sites). Moreover, the broad substrate specificity of rat Mrp2 might be achieved by combinations of the secondary binding sites (two electrostatically positive sites and two electrostatically negative sites) with the primary binding sites.

The method described here for determining the binding conformation of ligands represents a powerful tool in cases where ligands have the same binding mode to the target protein. Of course, it should be noted that different binding modes might exist for some ligands; however, all of the ligands used in this analysis appeared to have the same binding mode, according to the results of the CoMFA. We believe that our data will be useful in the development of new com-

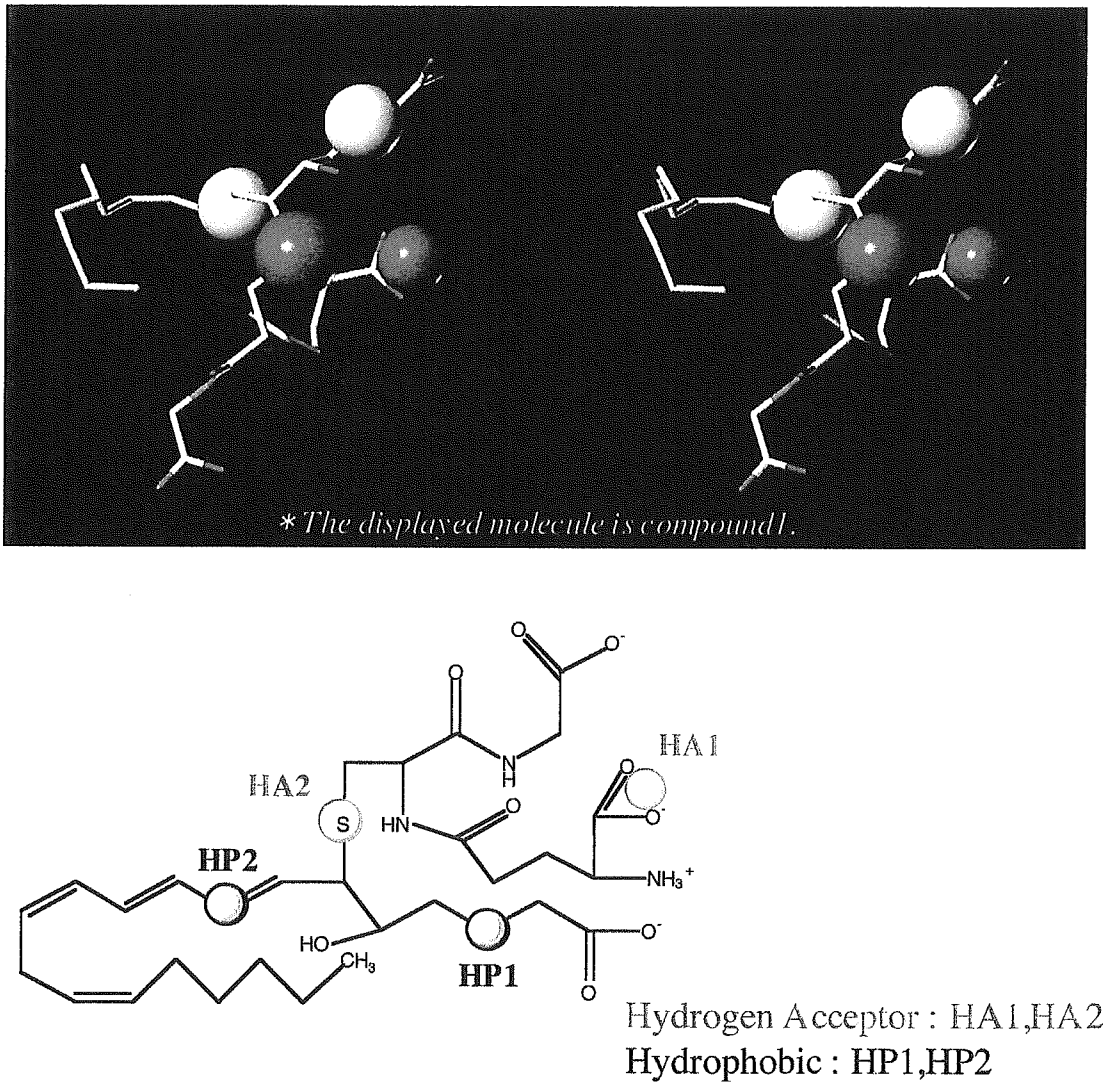

Fig. 7. A stereo view of the four property spheres that represent a 3D pharmacophore of ligands for Mrp2/ABCC2 and the 3D structure of compound **1** together with its structural formula.

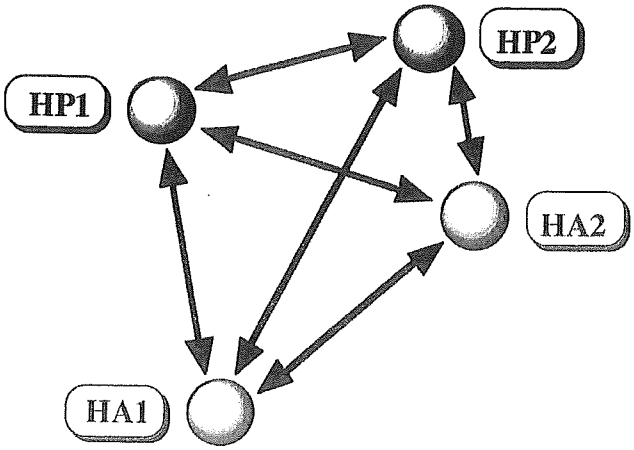

	Relative distances (Å)
HA1 - HA2	5.0 ± 0.9
HA1 - HP1	5.3 ± 0.7
HA1 - HP2	5.5 ± 1.6
HP1 - HA2	4.7 ± 0.8
HP1 - HP2	4.8 ± 1.1
HA2 - HP2	3.2 ± 1.2

Fig. 8. Relative distances between the four property spheres representing the functional groups that are essential for ligand binding.

compounds using the CoMFA QSAR model in order to evaluate their affinity for Mrp2.

REFERENCES

1. O. R. P. Elferink, D. K. Meijer, F. Kuipers, P. L. Jansen, A. K. Groen, and G. M. Groothuis. Hepatobiliary secretion of organic compounds; molecular mechanisms of membrane transport. *Biochim. Biophys. Acta* **1241**:215–268 (1995).
2. M. Yamazaki, H. Suzuki, and Y. Sugiyama. Recent advances in carrier-mediated hepatic uptake and biliary excretion of xenobiotics. *Pharm. Res.* **13**:497–513 (1996).
3. D. Keppler and J. Konig. Hepatic canalicular membrane 5: expression and localization of the conjugate export pump encoded by the *Mrp2* (*cMRP/cMOAT*) gene in liver. *FASEB J.* **11**:509–516 (1997).
4. K. Ito, H. Suzuki, T. Hirohashi, K. Kume, T. Shimizu, and Y. Sugiyama. Molecular cloning of canalicular multispecific organic anion transporter defective in EHBR. *Am. J. Physiol.* **272**:G16–G22 (1997).
5. C. C. Paulusma, P. J. Bosma, G. J. Zaman, C. T. Bakker, M. Otter, G. L. Scheffer, R. J. Scheper, P. Borst, and O. R. P. Elferink. Congenital jaundice in rats with a mutation in a multidrug resistance-associated protein gene. *Science* **271**:1126–1128 (1996).
6. K. Sathirakul, H. Suzuki, K. Yasuda, M. Hanano, O. Tagaya, T. Horie, and Y. Sugiyama. Kinetic analysis of hepatobiliary transport of organic anions in Eisai hyperbilirubinemic mutant rats. *J. Pharmacol. Exp. Ther.* **265**:1301–1312 (1993).
7. K. Sathirakul, H. Suzuki, T. Yamada, M. Hanano, and Y. Sugiyama. Multiple transport systems for organic anions across the bile canalicular membrane. *J. Pharmacol. Exp. Ther.* **268**:65–73 (1994).
8. M. Yamazaki, S. Akiyama, K. Ni'inuma, R. Nishigaki, and Y. Sugiyama. Biliary excretion of pravastatin in rats: contribution of the excretion pathway mediated by canalicular multispecific organic anion transporter. *Drug Metab. Dispos.* **25**:1123–1129 (1997).
9. H. Ishizuka, K. Konno, H. Naganuma, K. Sasahara, Y. Kawahara, K. Niinuma, H. Suzuki, and Y. Sugiyama. Temocaprilat, a novel angiotensin-converting enzyme inhibitor, is excreted in bile via an ATP-dependent active transporter (cMOAT) that is deficient in

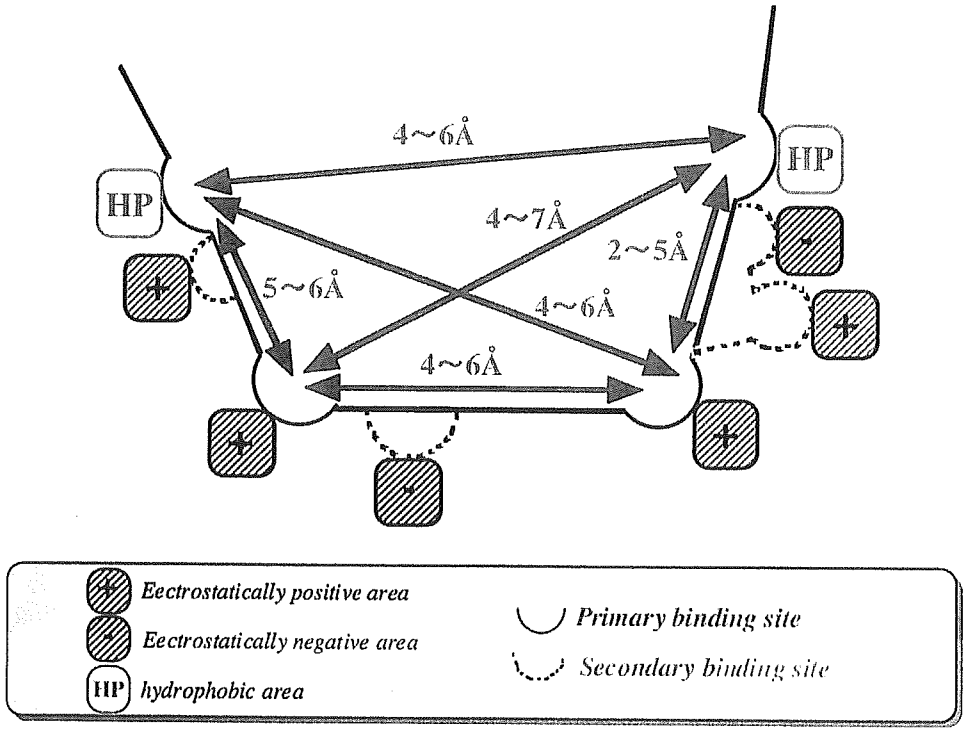

Fig. 9. Ligand-binding region of Mrp2/ABCC2 estimated using the 3D pharmacophore and CoMFA contour map.

Eisai hyperbilirubinemic mutant rats (EHBR). *J. Pharmacol. Exp. Ther.* **280**:1304–1311 (1997).
10. H. C. Shin, Y. Kato, T. Yamada, K. Niinuma, A. Hisaka, and Y. Sugiyama. Hepatobiliary transport mechanism for the cyclopentapeptide endothelin antagonist BQ-123. *Am. J. Physiol.* **272**: G979–G986 (1997).
11. T. Ishikawa, M. Muller, C. Klunemann, T. Schaub, and D. Keppler. ATP-dependent primary active transport of cysteinyl leukotrienes across liver canalicular membrane. Role of the ATP-dependent transport system for glutathione S-conjugates. *J. Biol. Chem.* **265**:19279–19286 (1990).
12. K. Kobayashi, Y. Sogame, H. Hara, and K. Hayashi. Mechanism of glutathione S-conjugate transport in canalicular and basolateral rat liver plasma membranes. *J. Biol. Chem.* **265**:7737–7741 (1990).
13. T. Nishida, Z. Gatmaitan, J. Roy-Chowdhry, and I. M. Arias. Two distinct mechanisms for bilirubin glucuronide transport by rat bile canalicular membrane vesicles. Demonstration of defective ATP-dependent transport in rats (TR-) with inherited conjugated hyperbilirubinemia. *J. Clin. Invest.* **90**:2130–2135 (1992).
14. O. Takenaka, T. Horie, K. Kobayashi, H. Suzuki, and Y. Sugiyama. Kinetic analysis of hepatobiliary transport for conjugated metabolites in the perfused liver of mutant rats (EHBR) with hereditary conjugated hyperbilirubinemia. *Pharm. Res.* **12**:1746–1755 (1995).
15. M. Trauner, M. Arrese, C. J. Soroka, M. Ananthanarayanan, T. A. Koeppel, S. F. Schlosser, F. J. Suchy, D. Keppler, and J. L. Boyer. The rat canalicular conjugate export pump (Mrp2) is down-regulated in intrahepatic and obstructive cholestasis. *Gastroenterology* **113**:255–264 (1997).
16. X. Y. Chu, Y. Kato, and Y. Sugiyama. Multiplicity of biliary excretion mechanisms for irinotecan, CPT-11, and its metabolites in rats. *Cancer Res.* **57**:1934–1938 (1997).
17. H. Suzuki and Y. Sugiyama. Role of transporters in the detoxification of xenobiotics: recent advances in the study of cMOAT/MRP. *Tanpakushitsu Kakusan Koso* **42**:1273–1284 (1997).
18. H. Tsujishita and S. Hirono. CAMDAS: an automated conformational analysis system using molecular dynamics. *J. Comput. Aided Mol. Des.* **11**:305–315 (1997).
19. K. Iwase and S. Hirono. Estimation of active conformations of drugs by a new molecular superposing procedure. *J. Comput. Aided Mol. Des.* **13**:499–512 (1999).
20. R. D. Cramer, D. E. Patterson, and J. D. Bunce. Comparative molecular field analysis (CoMFA). 1. Effect of shape on binding of steroids to carrier proteins. *J. Am. Chem. Soc.* **110**:5959–5967 (1988).
21. N. L. Allinger. Conformational analysis. 130. MM2. A hydrocarbon force field utilizing V1 and V2 torsional terms. *J. Am. Chem. Soc.* **99**:8127–8134 (1977).
22. H. Suzuki and Y. Sugiyama. Transporters for bile acids and organic anions. *Pharm. Biotechnol.* **12**:387–439 (1999).

Pharmaceutical Research, Vol. 22, No. 4, April 2005 (© 2005)
DOI: 10.1007/s11095-005-2502-1

Research Paper

Treatment of Hyperbilirubinemia in Eisai Hyperbilirubinemic Rat by Transfecting Human MRP2/ABCC2 Gene

Masakazu Hirouchi,[1] Hiroshi Suzuki,[1] and Yuichi Sugiyama[1,2]

Received October 8, 2004; accepted January 10, 2005

Purpose. Multidrug resistance–associated protein 2 (MRP2/ABCC2) is predominantly expressed in the liver canalicular membrane and plays an important role in the biliary excretion of organic anions including glucuronide and glutathione conjugates. The purpose of this study is to construct a new evaluation system for human MRP2 by expressing human MRP2 in Eisai hyperbilirubinemic rat (EHBR) liver, the rat Mrp2 function of which is hereditarily defective.
Methods. In order to express human MRP2 in liver, we used the Tet-off adenovirus expression system. After 72 h infection, we evaluated the protein expression and localization in the liver and the transport activity of [^{3}H]$E_2$17ßG and [^{3}H]DNP-SG by preparing canalicular membrane vesicles (CMVs). We also evaluated the biliary excretion and plasma concentration of DBSP after bolus administration and the plasma concentration of endogenous direct and indirect bilirubin.
Results. The localization of human MRP2 in EHBR liver was found to be at the bile canalicular membrane. Clear ATP-dependent uptake of [^{3}H]$E_2$17ßG and [^{3}H]DNP-SG into CMVs was observed by using the CMVs prepared from the liver where human MRP2 was transfected. Furthermore, the blood to bile clearance of DBSP increased approximately 3-fold after expression of human MRP2. In addition, the plasma direct bilirubin level in EHBR was reduced by the expression of human MRP2.
Conclusion. These results suggest that this evaluation system for human MRP2 may be useful for evaluating the function of human MRP2.

KEY WORDS: biliary excretion; EHBR; liver; MRP2.

INTRODUCTION

Multidrug resistance–associated protein 2 (MRP2/ABCC2) is a glycosylated integral plasma membrane protein belonging to the ATP-binding cassette transporter family. Its function has been studied extensively by comparing the transport across the bile canalicular membrane between normal and Mrp2-deficient mutant rats such as Eisai hyperbilirubinemic rats (EHBRs). Now, it is established that Mrp2 is mainly located on the bile canalicular membrane and the apical membrane of enterocytes and plays a primary role in biliary excretion and in restricting the oral absorption of its substrates, including anionic drugs and glutathione and glucuronide conjugates of xenobiotics (1–7). It has also been established that mutations in the MRP2 gene are responsible for the pathogenesis of Dubin-Johnson syndrome (DJS), characterized by a defect in the biliary excretion of bilirubin glucuronides (7–9). We have recently focused on the SNPs variants/mutants of MRP2, because, due to the fact that some MRP2 mutations found in DJS patients are associated with a loss of transport activity and/or the ability to traffick to the apical membrane by the single amino acid alteration (10,11), it is possible that the MRP2 SNPs may also be associated with alterations in function and, consequently, may be responsible for the inter-individual differences in the disposition of substrate drugs. Previously, we have characterized the function of SNPs variants/mutants of MRP2 using LLC-PK1 cells (12). Although the wild-type MRP2 was exclusively localized at the apical membrane, S789F and A1450T MRP2 were located not only at the apical membrane but also in the intracellular compartment, suggesting that the *in vivo* function of these two kinds of variants may be lower than wild type MRP2 (12).

However, there are some reports which suggest that the localization of some membrane proteins in cultured cells does not necessarily reflect the localization in tissues. For example, rat Oat-K1 is localized at the apical membrane in the proximal tubules (13), whereas this transporter localizes at the basolateral membrane in LLC-PK1 cells, derived from porcine kidney (14). Moreover, rat serotonin transporter and norepinephrine transporter are known to be sorted to the apical compartment (axolemmal domain) of neuronal cells, whereas these transporters are sorted to the basolateral membrane in MDCK cells, derived from canine kidney (15). One

[1] School of Pharmaceutical Sciences, University of Tokyo, Hongo, Bunkyo-ku, Tokyo 113-0033, Japan.
[2] To whom correspondence should be addressed. (e-mail: sugiyama@mol.f.u-tokyo.ac.jp)

ABBREVIATIONS: Ad, adenovirus; CMV, canalicular membrane vesicle; DBSP, dibromosulfophtalein; DJS, Dubin-Johnson syndrome; DNP-SG, 2,4-dinitrophenyl-*S* glutathione; $E_2$17ßG, 17β-estradiol 17β-D-glucuronide; EHBR, Eisai hyperbilirubinemic rats; MRP, multidrug resistance–associated protein; pfu, plaque-forming unit; SNPs, single nucleotide polymorphisms; TRE, tet-responsive element; tTA, tetracycline-responsive transcriptional activator.

of the hypotheses for these alterations of the cellular localization is that some proteins which are necessary for the apical targeting under physiologic conditions are deficient in cultured cells. Concerning this point, it is essential to determine the localization of SNPs variants/mutants of MRP2 in human liver, although such determination is quite difficult. Therefore, we have planned to construct an *in vitro* evaluation system which may reflect the cellular localization under physiologic conditions. Thus, we have focused on using the Eisai hyperbilirubinemic rat (EHBR), as the mutation in the Mrp2 gene leads to the absence of Mrp2 protein in this mutant strain (16,17).

The purpose of this study is to establish a new system for evaluating the function of human MRP2 by expressing this transporter on the canalicular membrane of EHBR liver. To express human MRP2 in EHBR liver, we used Tet-off recombinant adenovirus systems. The expression level, localization and the transport function of human MRP2 in EHBR liver were analyzed.

MATERIALS AND METHODS

Materials

[^{3}H]$E_2$17ßG (51.0 μCi/nmol) with a purity of 98.5% was purchased from New England Nuclear (Boston, MA, USA). Unlabeled and [^{3}H]labeled 2,4-dinitrophenyl-*S*-glutathione ([^{3}H]DNP-SG, 44.8 μCi/nmol) were synthesized as described previously (18). ATP, creatine phosphate, creatine phosphokinase, acivicin, and glutathione *S*-transferase were purchased from Sigma Chemical (St. Louis, MO, USA). All other chemicals used were commercially available and of reagent grade. Sprague-Dawley rats (normal rats) and EHBR weighing approximately 180 g were used throughout the experiments.

Construction of Recombinant Adenoviruses Containing MRP2

Human MRP2 cDNA located between the Not I and Nco I sites of pBluescript SK(-) (Stratagene, La Jolla, CA, USA) was provided by Dr. Kuwano (Kyushu University School of Medicine). The MRP2 cDNA was subcloned into the Not I and Nco I sites of the pTRE shuttle, resulting in the production of pTRE shuttle-MRP2. pTRE shuttle-MRP2 has I-CeuI and PI-SceI sites upstream and downstream of the MRP2 expression cassette, respectively. The I-CeuI / PI-SceI digested fragments of pTRE shuttle-MRP2 were ligated with I-CeuI / PI-SceI digested Adeno-X Viral DNA (BD Biosciences, Palo Alto, CA, USA), resulting in pAd-MRP2. pAd containing tetracycline-responsive transcriptional activator (tTA) (pAd-tTA) was purchased from Clontech (Palo Alto, CA, USA).

To generate the recombinant viruses, both pAd-MRP2 and pAd-tTA were digested with PacI. Linearized DNAs were transfected to HEK293 cells grown on a 12-well dish with Fugene 6 (Roche Diagnostics Corp., Tokyo, Japan) according to the manufacturer's instructions. Viruses (Ad-MRP2 and Ad-tTA) were prepared as described previously (19). Recombinant viruses were purified by CsCl gradient centrifugation, dialyzed with a solution containing 10 mM Tris (pH 7.5), 1 mM $MgCl_2$, and 10% glycerol, and stored in aliquots at −80°C. Then, the resulting virus titer was determined as described previously (20).

Infection of Recombinant Adenovirus and the Preparation of Canalicular Membrane Vesicles

The adenoviruses were injected to EHBR via the tail vein. EHBR were infected with both Ad-MRP2 and Ad-tTA to express human MRP2 (MRP2-EHBR). For the negative control, EHBR were infected only with Ad-tTA (control EHBR). CMVs were prepared from EHBR liver 72 h after adenovirus infection as described previously (18) and kept as a suspension in 50 mM Tris buffer (pH 7.4) containing 250 mM sucrose. The membrane vesicles were frozen in liquid N_2 and stored at −80°C until required. The activity of the CMVs was checked by measuring the ATP-dependent uptake of standard substrates, [^{3}H]$E_2$17ßG (400 nM) and [^{3}H]DNP-SG (1 μM) for a 5-min incubation at 37°C. Protein concentrations were determined by the Lowry method.

Immunoblots

For the Western blot analysis, CMVs were dissolved in 3x SDS sample buffer (New England BioLabs, Beverly, MA, USA) and subjected to electrophoresis on a 7% SDS-polyacrylamide gel with a 4.4% stacking gel. The molecular weight was determined using a prestained protein marker (New England BioLabs). Proteins were transferred electrophoretically to a nitrocellulose membrane (Millipore, Bedford, MA, USA) using a blotter (Bio-Rad Laboratories, Richmond, CA, USA) at 15 V for 1 h The membrane was blocked with 2.5% skimmed milk for 1 h at room temperature. Then, the membrane was incubated for 40 min at room temperature with anti-MRP2 rabbit serum, diluted with skimmed milk (1:500), which was raised against 12 amino acids at the carboxyl terminus of the deduced MRP2 sequence (EAGIENVNSTKF). For the detection of MRP2, the membrane was allowed to bind to Alexa Fluor 680 goat anti-rabbit IgG (H+L) (Molecular Probes, Inc., Eugene, OR, USA). The fluorescence was assessed in a densitometer (Odyssey, ALOKA, Tokyo, Japan).

Immunofluorescence

For the immunofluorescence, liver from MRP2-EHBR and control-EHBR was removed 72 h after infection. Cryostat sections (5 μm in thickness) were fixed in methanol at −20°C for 10 min, washed three times with PBS, and blocked with 1% BSA/PBS at room temperature for 15 min. Then, slices were incubated with the monoclonal antibody against MRP2 (M2-6 (Molecular Probes Inc., Eugene, OR, USA), diluted 40-fold in PBS) for 1 h at room temperature. Following this, slices were washed three times with PBS and incubated with goat anti-mouse IgG Alexa 488 (Molecular Probes, Inc.) diluted 250-fold in PBS for 1 h at room temperature, and mounted in VECTASHIELD Mounting Medium (Vector Laboratories, Burlingame, CA, USA). The localization of the MRP2 protein was visualized by confocal laser microscopy (Zeiss LSM-510; Carl Zeiss Inc., Thornwood, NY, USA).

Vesicle Transport Assays

The uptake study of [^{3}H]$E_2$17ßG (400 nM) and [^{3}H]DNP-SG (1 μM) was performed as reported previously (21). Briefly, the transport medium (10 mM Tris, 250 mM sucrose and 10 mM $MgCl_2 \cdot 6H_2O$, pH 7.4) contained the ligands, 5 mM ATP, and an ATP-regenerating system (10 mM creatine phosphate and 100 μg/ml of creatine phosphokinase). An aliquot of transport medium (17–18 μl) was mixed rapidly with the vesicle suspension (5 μg protein in 2–3 μl). The transport reaction was stopped by the addition of 1 ml ice-cold buffer containing 250 mM sucrose, 0.1 M NaCl and 10 mM Tris-HCl (pH 7.4). The stopped reaction mixture was filtered through 0.45-μm HA filters (Millipore Corp.) and then washed twice with 5 ml of the stop solution. The radioactivity retained on the filter was measured in a liquid scintillation counter (LS 6000SE, Beckman Instruments, Fullerton, CA, USA) after the addition of scintillation cocktail (Clear-sol I, Nacarai Tesque, Tokyo, Japan). Ligand uptake was normalized in terms of the amount of membrane protein.

Blood and Bile Sampling

Sprague-Dawley rats (normal rats) and EHBR were kept under ether anesthesia and then the femoral artery and vein were cannulated with polyethylene tubing (PE-50) for ligand administration and blood sampling, respectively. The common bile duct was also cannulated with PE-10. DBSP (10 μmol/kg) in saline was administered intravenously through the femoral vein cannula. Blood samples were obtained at given times. The rectal temperature was maintained at 37°C ± 0.5°C with a heat lamp.

Analysis of Specimens Obtained from *in Vivo* Experiments

To determine the DBSP concentrations, plasma and bile specimens were diluted with 50 mM Tris-HCl buffer (pH 7.4) free from bovine serum albumin, and then made alkaline by the addition of NaOH. Concentrations of DBSP in the diluted specimens were determined in a dual-wave length spectrophotometer (Hitachi Ltd., Tokyo, Japan) at a wavelength of 575 nm/620 nm. Direct and indirect bilirubin concentrations of some specimens were also determined using a test kit (Bilirubin BII-Test Wako, Wako Pure Chemical Industries, Ltd., Tokyo, Japan). Bile volume was measured gravimetrically, assuming a density of 1.0 for bile specimens.

RESULTS

Expression Level of MRP2 Protein in EHBR Liver

To determine the appropriate amount of adenoviruses for the protein expression of human MRP2 in EHBR liver, 1×10^9, 7.5×10^9, 1×10^{10}, and 2.5×10^{10} plaque-forming units (pfu) of both Ad-MRP2 and Ad-tTA were injected to EHBR through the tail vein. Presumably due to the liver toxicity of the viruses, EHBR infected with 1×10^{10} and 2.5×10^{10} pfu died soon after injection. The expression level of human MRP2 in the canalicular membrane fraction isolated from EHBR liver was examined by Western blot analysis. It was found that the human MRP2 antibody recognized the band with an approximate molecular weight of 190 kDa (Fig. 1), which is consistent with a previous report (22). When infected

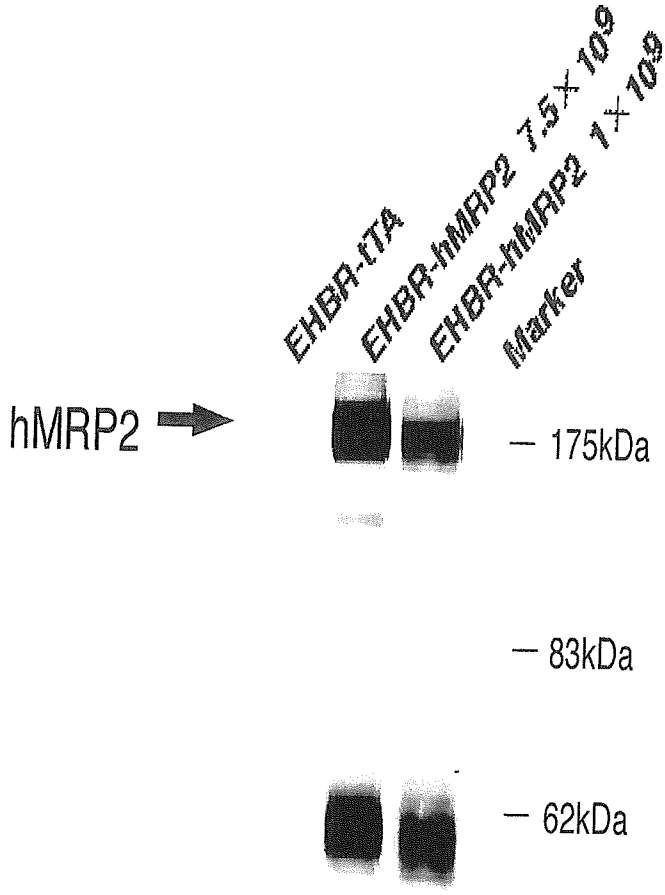

Fig. 1. Expression of human MRP2 in CMVs. Expression of the human MRP2 protein was determined in CMVs (5 μg) isolated from control-EHBR and MRP2-EHBR by Western blot analysis.

with 7.5×10^9 pfu, the band density of MRP2 was approximately 5-fold higher compared with that in EHBR infected with 1×10^9 pfu (Fig. 1).

Localization of Human MRP2 in EHBR Liver

The localization of human MRP2 in EHBR liver was determined by immunofluorescence. Using an antibody against MRP2, the fluorescence signal was detected exclusively at the bile canalicular membrane of EHBR liver after simultaneous infection of Ad-tTA and Ad-MRP2 (Fig. 2). No

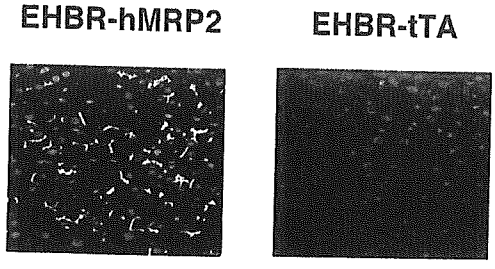

Fig. 2. Localization of human MRP2 in EHBR liver. The immunolocalization of MRP2 molecules in MRP2-EHBR was determined using a monoclonal antibody for human MRP2 (green). Nuclei were stained with PI (red).

specific fluorescence signal of MRP2 was observed in the EHBR liver after infection of only Ad-tTA (Fig. 2).

Transport Activity Associated with the Isolated CMVs

After confirming the protein expression level of MRP2, the uptake of MRP2 substrates was examined using thr isolated CMVs. Typical substrates of MRP2, [^{3}H]$E_2$17ßG and [^{3}H]DNP-SG, were clearly taken up into CMVs prepared from MRP2-EHBR in an ATP-dependent manner (Fig. 3). In particular, the ATP-dependent uptake of CMVs was higher when infected with 7.5×10^9 pfu than with 1.0×10^9 pfu, which is consistent with the result of the Western blot analysis (Fig. 1). Moreover, the extent of the uptake of [^{3}H]$E_2$17ßG and [^{3}H]DNP-SG was almost identical to that of the CMVs prepared from normal SD rats when infected with 7.5×10^9 pfu of Ad-MRP2 (Fig. 3).

Biliary Excretion of DBSP

The plasma disappearance of DBSP was compared between control-EHBR and MRP2-EHBR. Figure 4A shows that the plasma disappearance curves for DBSP after *i.v.* administration were similar for control-EHBR and MRP2-EHBR up to 21 min. In contrast, the maximum biliary excretion rate in MRP2-EHBR was approximately 3-fold higher than that in control-EHBR (Fig. 4B). The cumulative amount of DBSP excreted into the bile up to 2 h in MRP2-EHBR was greater than that in control-EHBR (Fig. 4C). The biliary excretion clearance value, defined by dividing the total amount excreted into bile by AUC of DBSP, in MRP2-EHBR in creased 3-fold compared with that in control-EHBR (Table I).

Bilirubin Concentration in Serum and Bile

The concentration of both direct and indirect bilirubin in the serum of normal rats, EHBR, control-EHBR, and MRP2-EHBR was also measured. The concentration of both direct and indirect bilirubin in the serum was significantly lower in MRP2-EHBR compared with control-EHBR (7.1 mg/ml vs. 97.4 mg/ml) (Table I). The decrease in direct bilirubin after

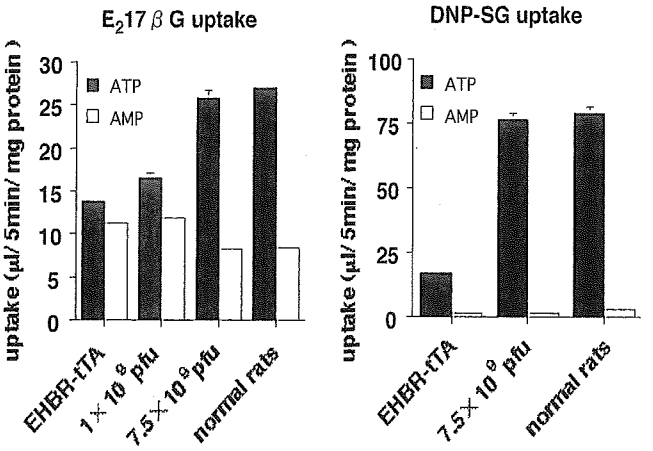

Fig. 3. Transport activity of human MRP2 in CMVs. [^{3}H]$E_2$17ßG and [^{3}H]DNP-SG uptake was measured in CMVs from MRP2-EHBR and control-EHBR. CMVs were incubated at 37°C with [^{3}H]$E_2$17ßG (400 nM) and [^{3}H]DNP-SG (500 nM) in the medium containing ATP (solid bar) and AMP (open bar) for 5 min. The results are shown as the mean ± SE of triplicate determinations.

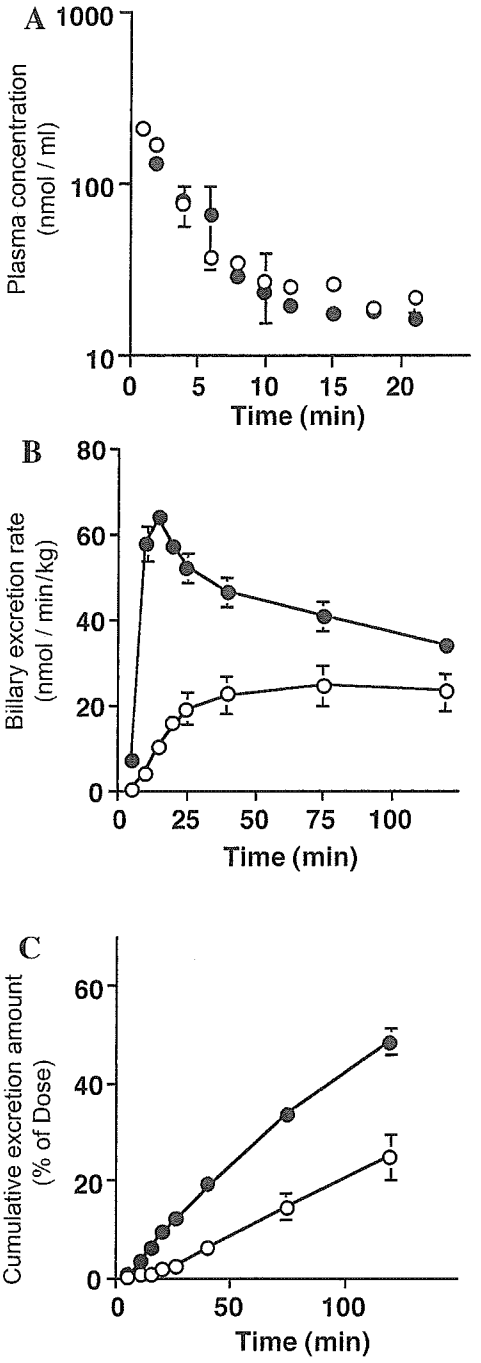

Fig. 4. Biliary excretion of DBSP. DBSP (10 μmol/kg) was administered intravenously as a bolus to MRP2-EHBR (●) and control-EHBR (○). (A) shows the plasma disappearance curves for DBSP. (B) and (C) show the time-course for the biliary excretion rate and that for cumulative biliary excretion, respectively. Each point and bar represents the mean ± SE of 3 rats.

human MRP2 expression was much greater than that in indirect bilirubin (from 97.4 mg/ml to 7.1 mg/ml, vs. 10.8 mg/ml to 4.9 mg/ml) (Table I), presumably because the direct bilirubin can be excreted into bile via human MRP2 (23). However, the concentration of direct bilirubin in control-EHBR plasma was much greater than that in untreated EHBR (97.4 mg/ml vs. 30.1 mg/ml) (Table I). In our preliminary results, infection of adenoviruses induced the expression of Mrp3, which is ex-

Table I. Bile Flow Rate, Concentration of Bilirubin in Serum, and the Biliary Excretion Clearance of DBSP

	SD rat	MRP2-EHBR	Control-EHBR	EHBR
Bile flow rate ($\mu l\ min^{-1}\ g\ liver^{-1}$)	1.14 ± 0.10	1.08 ± 0.13	0.79 ± 0.10	0.79 ± 0.08
Serum bilirubin (μM)				
Direct	1.0 ± 0.5	7.1 ± 0.9**	97.4 ± 8.2	30.1 ± 4.5
Indirect	1.1 ± 0.5	4.9 ± 2.3	10.8 ± 1.7	6.2 ± 3.2
CL_H ($ml\ min^{-1}\ kg^{-1}$)	32.1 ± 7.8	3.2 ± 0.5*	1.1 ± 0.2	2.4 ± 0.2

The biliary excretion clearance of DBSP are analyzed from the data of Fig. 4.
* $p < 0.05$ vs. control-EHBR; **$p < 0.01$ vs. control-EHBR by student's t-test.

pressed at the sinusoidal membrane of the liver. Since direct bilirubin can be excreted into blood via Mrp3 (24), the increase in the plasma direct bilirubin levels in control-EHBR may be accounted for by the increase of sinusoidal Mrp3 expression induced by adenovirus infection.

DISCUSSION

The function of Mrp2/MRP2 has been studied extensively by comparing the transport across the bile canalicular membrane between normal and Mrp2-deficient rats (such as Groningen Yellow (GY), transport deficient (TR-), and Eisai hyperbilirubinemic rats (EHBRs)) (16,17,25,26). Furthermore, MRP2 function has been characterized by using the cDNA-transfected cells (1,3,6,22). The canalicular localization of MRP2 (23) has been reflected by the apical localization in polarized mammalian cell lines (22). It is also reported that the pathogenesis of some DJS is accounted for by the lack in the normal apical sorting of MRP2 molecules (10,11). The localization of MRP2 have been characterized by the polarized mammalian cell lines (22), and by the liver sample from DJS patients (10,11). Moreover, we have analyzed the function of MRP2 SNPs variants/mutants using the LLC-PK1 cell line, and found that some variants were localized not only at the apical membrane but also in the intracellular compartment of this polarized cell line (12). Since the SNPs/mutations of MRP2 may have an effect on drug disposition, identification of the *in vivo* localization of MRP2 variants is quite important. In the current study, we have constructed a model for evaluating the function of human MRP2 using EHBR.

We first investigated whether the localization of human MRP2 in liver is preserved in EHBR or not. The human MRP2 was expressed on the canalicular membrane after the adenovirus infection (Fig. 2), which is consistent with the physiologic localization of rat and human MRP2 (23), suggesting that the sorting mechanism of human MRP2 is also present in rat liver. Although we were unable to compare the absolute value of MRP2 protein expression between normal rats (rat MRP2) and MRP2-EHBR (human MRP2), the transport activity of CMVs from normal rats and MRP2-EHBR infected with 7.5×10^9 pfu was almost identical after the normalization of the membrane protein amount of CMVs (Fig. 3), suggesting that the expression level of human MPR2 may be enough for performing the *in vivo* experiments.

From the uptake study with CMVs, we are only able to estimate the drug transport from the liver across the bile canalicular membrane, whereas by performing the *in vivo* study, we are also able to evaluate the vectorical transport of drugs from blood to bile, which is essential for estimating the *in vivo* human biliary excretion. We have previously suggested that the biliary excretion of DBSP is reduced in EHBR compared with that in normal rats *in vivo* (27). Moreover, from the kinetic analysis, the reduction in the biliary excretion of organic anions may be due to a defect in the transport carriers on the bile canalicular membrane (27), suggesting that DBSP is predominantly excreted into bile via MRP2. Therefore, we selected DBSP as a model compound for examining its biliary excretion in a bolus infusion study. After iv injection of DBSP, the plasma concentration was similar between control-EHBR and MRP2-EHBR (Fig. 4A). Because the initial elimination of DBSP from plasma represents the hepatic uptake of this dye (27), this result suggests that the hepatic uptake activity is comparable between control-EHBR and MRP2-EHBR. However, a significant difference in the biliary excretion rate and that in the cumulative excretion were observed (Figs. 4B and 4C), suggesting that human MRP2 introduced by adenovirus recognizes DBSP as a substrate, and excretes DBSP from liver to bile via human MRP2. Moreover, the serum concentration of direct bilirubin was greatly reduced in MRP2-EHBR compared with that in control EHBR (Table I). This result suggests that human MRP2 excretes direct bilirubin into bile, resulting in an improvement of the symptoms of hyperbilirubinemia. However, the biliary excretion clearance in DBSP by MRP2-EHBR was only 3-fold of that of control-EHBR (Table I). It was in contrast to the fact that the biliary excretion clearance of DBSP was 10-fold higher in normal rats than that in EHBR, which is consistent with our previous result (27). Because the result of the *in vitro* transport activity for $E_2$17ßG and DNP-SG indicated that the expression level of human MRP2 is high enough (Fig. 3), we expected that the biliary excretion clearance of DBSP would be comparable between normal rats and MRP2-EHBR. This unexpected finding can be explained by considering the induction of sinusoidal Mrp3 by the adenovirus infection. It is possible that DBSP is excreted into blood via Mrp3, as a similar substrate specificity of Mrp2 and Mrp3 has been reported (28–30). The fact that the serum concentration of direct bilirubin was much greater in control-EHBR than that in untreated EHBR (97.4 mg/ml vs. 30.1 mg/ml) (Table I), may also be explained by Mrp3 induction by infection with the adenoviruses. Alternatively, the transport activity of DBSP by human MRP2 is lower than that by rat Mrp2, resulting the lower biliary excretion clearance of DBSP by MRP2-EHBR compared with normal rats.

In conclusion, we have been able to express human MRP2 at the canalicular membrane in EHBR liver. By comparing the expression level of MRP2 between MRP2-EHBR

and in human liver, this system may be useful in quantatively predicting the *in vivo* human biliary excretion of human MRP2 substrates. Moreover, because the wild-type human MRP2 was expressed at the canalicular membrane of EHBR liver, it may be possible to predict the localization and function of SNPs variants/mutants of human MRP2 in the intact liver.

REFERENCES

1. H. Suzuki and Y. Sugiyama. Transporters for bile acids and organic anions. *Pharm. Biotechnol.* **12**:387–439 (1999).
2. Y. Gotoh, H. Suzuki, S. Kinoshita, T. Hirohashi, Y. Kato, and Y. Sugiyama. Involvement of an organic anion transporter (canalicular multispecific organic anion transporter/multidrug resistance-associated protein 2) in gastrointestinal secretion of glutathione conjugates in rats. *J. Pharmacol. Exp. Ther.* **292**:433–439 (2000).
3. D. Keppler and J. Konig. Hepatic secretion of conjugated drugs and endogenous substances. *Semin. Liver Dis.* **20**:265–272 (2000).
4. H. Suzuki and Y. Sugiyama. Role of metabolic enzymes and efflux transporters in the absorption of drugs from the small intestine. *Eur. J. Pharm. Sci.* **12**:3–12 (2000).
5. C. G. Dietrich, D. R. de Waart, R. Ottenhoff, I. G. Schoots, and R. P. Elferink. Increased bioavailability of the food-derived carcinogen 2-amino-1-methyl-6-phenylimidazo[4,5-b]pyridine in MRP2-deficient rats. *Mol. Pharmacol.* **59**:974–980 (2001).
6. L. Payen, L. Sparfel, A. Courtois, L. Vernhet, A. Guillouzo, and O. Fardel. The drug efflux pump MRP2: regulation of expression in physiopathological situations and by endogenous and exogenous compounds. *Cell Biol. Toxicol.* **18**:221–233 (2002).
7. H. Suzuki and Y. Sugiyama. Single nucleotide polymorphisms in multidrug resistance associated protein 2 (MRP2/ABCC2): its impact on drug disposition. *Adv. Drug Deliv. Rev.* **54**:1311–1331 (2002).
8. P. Borst and R. O. Elferink. Mammalian ABC transporters in health and disease. *Annu. Rev. Biochem.* **71**:537–592 (2002).
9. R. O. Elferink and A. K. Groen. Genetic defects in hepatobiliary transport. *Biochim. Biophys. Acta* **1586**:129–145 (2002).
10. V. Keitel, J. Kartenbeck, A. T. Nies, H. Spring, M. Brom, and D. Keppler. Impaired protein maturation of the conjugate export pump multidrug resistance protein 2 as a consequence of a deletion mutation in Dubin-Johnson syndrome. *Hepatology* **32**:1317–1328 (2000).
11. K. Hashimoto, T. Uchiumi, T. Konno, T. Ebihara, T. Nakamura, M. Wada, S. Sakisaka, F. Maniwa, T. Amachi, K. Ueda, and M. Kuwano. Trafficking and functional defects by mutations of the ATP-binding domains in MRP2 in patients with Dubin-Johnson syndrome. *Hepatology* **36**:1236–1245 (2002).
12. M. Hirouchi, H. Suzuki, and Y. Sugiyama. Characterization of the cellular localization, expression level, and function of SNP variants of MRP2/ABCC2. *Pharm. Res.* **12**:387–439 (2004).
13. S. Masuda, K. Ibaramoto, A. Takeuchi, H. Saito, Y. Hashimoto, and K. I. Inui. Cloning and functional characterization of a new multispecific organic anion transporter, OAT-K2, in rat kidney. *Mol. Pharmacol.* **55**:743–752 (1999).
14. S. Masuda, H. Saito, and K. I. Inui. Interactions of nonsteroidal anti-inflammatory drugs with rat renal organic anion transporter, OAT-K1. *J. Pharmacol. Exp. Ther.* **283**:1039–1042 (1997).
15. H. H. Gu, J. Ahn, M. J. Caplan, R. D. Blakely, A. I. Levey, and G. Rudnick. Cell-specific sorting of biogenic amine transporters expressed in epithelial cells. *J. Biol. Chem.* **271**:18100–18106 (1996).
16. M. Buchler, J. Konig, M. Brom, J. Kartenbeck, H. Spring, T. Horie, and D. Keppler. cDNA cloning of the hepatocyte canalicular isoform of the multidrug resistance protein, cMrp, reveals a novel conjugate export pump deficient in hyperbilirubinemic mutant rats. *J. Biol. Chem.* **271**:15091–15098 (1996).
17. K. Ito, H. Suzuki, T. Hirohashi, K. Kume, T. Shimizu, and Y. Sugiyama. Molecular cloning of canalicular multispecific organic anion transporter defective in EHBR. *Am. J. Physiol.* **272**: G16–G22 (1997).
18. K. Kobayashi, Y. Sogame, H. Hara, and K. Hayashi. Mechanism of glutathione S-conjugate transport in canalicular and basolateral rat liver plasma membranes. *J. Biol. Chem.* **265**:7737–7741 (1990).
19. H. Mizuguchi and M. A. Kay. Efficient construction of a recombinant adenovirus vector by an improved in vitro ligation method. *Hum. Gene Ther.* **9**:2577–2583 (1998).
20. H. Mizuguchi and M. A. Kay. A simple method for constructing E1- and E1/E4-deleted recombinant adenoviral vectors. *Hum. Gene Ther.* **10**:2013–2017 (1999).
21. T. Hirohashi, H. Suzuki, X. Y. Chu, I. Tamai, A. Tsuji, and Y. Sugiyama. Function and expression of multidrug resistance-associated protein family in human colon adenocarcinoma cells (Caco-2). *J. Pharmacol. Exp. Ther.* **292**:265–270 (2000).
22. R. Evers, M. Kool, L. van Deemter, H. Janssen, J. Calafat, L. C. Oomen, C. C. Paulusma, R. P. Oude Elferink, F. Baas, A. H. Schinkel, and P. Borst. Drug export activity of the human canalicular multispecific organic anion transporter in polarized kidney MDCK cells expressing cMOAT (MRP2) cDNA. *J. Clin. Invest.* **101**:1310–1319 (1998).
23. D. Keppler, J. Konig, and M. Buchler. The canalicular multidrug resistance protein, cMRP/MRP2, a novel conjugate export pump expressed in the apical membrane of hepatocytes. *Adv. Enzyme Regul.* **37**:321–333 (1997).
24. T. Kamisako, Y. Kobayashi, K. Takeuchi, T. Ishihara, K. Higuchi, Y. Tanaka, E. C. Gabazza, and Y. Adachi. Recent advances in bilirubin metabolism research: the molecular mechanism of hepatocyte bilirubin transport and its clinical relevance. *J. Gastroenterol.* **35**:659–664 (2000).
25. R. Mayer, J. Kartenbeck, M. Buchler, G. Jedlitschky, I. Leier, and D. Keppler. Expression of the MRP gene-encoded conjugate export pump in liver and its selective absence from the canalicular membrane in transport-deficient mutant hepatocytes. *J. Cell Biol.* **131**:137–150 (1995).
26. C. C. Paulusma, P. J. Bosma, G. J. Zaman, C. T. Bakker, M. Otter, G. L. Scheffer, R. J. Scheper, P. Borst, and R. P. Oude Elferink. Congenital jaundice in rats with a mutation in a multidrug resistance-associated protein gene. *Science* **271**:1126–1128 (1996).
27. K. Sathirakul, H. Suzuki, K. Yasuda, M. Hanano, O. Tagaya, T. Horie, and Y. Sugiyama. Kinetic analysis of hepatobiliary transport of organic anions in Eisai hyperbilirubinemic mutant rats. *J. Pharmacol. Exp. Ther.* **265**:1301–1312 (1993).
28. H. Akita, H. Suzuki, T. Hirohashi, H. Takikawa, and Y. Sugiyama. Transport activity of human MRP3 expressed in Sf9 cells: comparative studies with rat MRP3. *Pharm. Res.* **19**:34–41 (2002).
29. T. Hirohashi, H. Suzuki, H. Takikawa, and Y. Sugiyama. ATP-dependent transport of bile salts by rat multidrug resistance-associated protein 3 (Mrp3). *J. Biol. Chem.* **275**:2905–2910 (2000).
30. J. Konig, A. T. Nies, Y. Cui, I. Leier, and D. Keppler. Conjugate export pumps of the multidrug resistance protein (MRP) family: localization, substrate specificity, and MRP2-mediated drug resistance. *Biochim. Biophys. Acta* **1461**:377–394 (1999).

0022-3565/05/3143-1059–1067$20.00
THE JOURNAL OF PHARMACOLOGY AND EXPERIMENTAL THERAPEUTICS

JPET 314:1059–1067, 2005

Vol. 314, No. 3
85589/3044446
Printed in U.S.A.

Identification of the Hepatic Efflux Transporters of Organic Anions Using Double-Transfected Madin-Darby Canine Kidney II Cells Expressing Human Organic Anion-Transporting Polypeptide 1B1 (OATP1B1)/Multidrug Resistance-Associated Protein 2, OATP1B1/Multidrug Resistance 1, and OATP1B1/Breast Cancer Resistance Protein

Soichiro Matsushima, Kazuya Maeda, Chihiro Kondo, Masaru Hirano, Makoto Sasaki, Hiroshi Suzuki, and Yuichi Sugiyama

Graduate School of Pharmaceutical Sciences, The University of Tokyo, Bunkyo-ku, Tokyo, Japan

Received February 28, 2005; accepted May 17, 2005

ABSTRACT

Until recently, it was generally believed that the transport of various organic anions across the bile canalicular membrane was mainly mediated by multidrug resistance-associated protein 2 (MRP2/ABCC2). However, a number of new reports have shown that some organic anions are also substrates of multidrug resistance 1 (MDR1/ABCB1) and/or breast cancer resistance protein (BCRP/ABCG2), implying MDR1 and BCRP could also be involved in the biliary excretion of organic anions in humans. In the present study, we constructed new double-transfected Madin-Darby canine kidney II (MDCKII) cells expressing organic anion-transporting polypeptide 1B1 (OATP1B1)/MDR1 and OATP1B1/BCRP, and we investigated the transcellular transport of four kinds of organic anions, estradiol-17β-D-glucuronide (EG), estrone-3-sulfate (ES), pravastatin (PRA), and cerivastatin (CER), to identify which efflux transporters mediate the biliary excretion of compounds using double-transfected cells. We observed the vectorial transport of EG and ES in all the double transfectants. MRP2 showed the highest efflux clearance of EG among these efflux transporters, whereas BCRP-mediated clearance of ES was the highest in these double transfectants. In addition, two kinds of 3-hydroxy-3-methylglutaryl-CoA reductase inhibitors, CER and PRA, were also substrates of all these efflux transporters. The rank order of the efflux clearance of PRA mediated by each transporter was the same as that of EG, whereas the contribution of MDR1 to the efflux of CER was relatively greater than for PRA. This experimental system is very useful for identifying which transporters are involved in the biliary excretion of organic anions that cannot easily penetrate the plasma membrane.

Biliary excretion is one of the major pathways for the elimination of unnecessary compounds from blood circulation. In the common process of hepatic clearance, compounds are taken up into liver, converted to more hydrophilic metabolites by metabolizing enzymes responsible for oxidation (e.g., cytochrome P450) and/or conjugation (e.g., UDP-glucuronosyl transferases and sulfotransferases), and subsequently excreted into bile. Several kinds of ATP-binding cassette (ABC) transporters on the bile canalicular membrane play an important role in this biliary excretion. It is generally accepted that multidrug resistance-associated protein 2 (MRP2/ABCC2) is responsible for the biliary excretion of a wide variety of organic anions including glutathione and glucuronide conjugates (Suzuki and Sugiyama, 1998; Konig et al., 1999). This has been proven by comparing the transport activity across the bile canalicular membrane between

This study was supported by Health and Labor Sciences Research grants from the Ministry of Health, Labor, and Welfare for the Research on Advanced Medical Technology and by Grant-in-Aid for Young Scientists B (15790087) from the Ministry of Education, Culture, Sports, Science, and Technology.

Article, publication date, and citation information can be found at http://jpet.aspetjournals.org.

doi:10.1124/jpet.105.085589.

ABBREVIATIONS: ABC, ATP-binding cassette; MRP, multidrug resistance-associated protein; EHBR, Eisai hyperbilirubinemic rats; MDR, multidrug resistance; EG, estradiol-17β-D-glucuronide; E3040, 6-hydroxy-5,7-dimethyl-2-methylamino-4-(3-pyridylmethyl) benzothiazole; BCRP, breast cancer resistance protein; MDCK, Madin-Darby canine kidney; OATP, organic anion-transporting polypeptide; PRA, pravastatin; HMG, 3-hydroxy-3-methylglutaryl; ES, estrone-3-sulfate; CER, cerivastatin; PBS, phosphate-buffered saline; TTBS, Tris-buffered saline with 0.05% Tween 20; PS, permeability surface product.

normal and Mrp2-deficient rats such as Eisai hyperbilirubinemic rats (EHBR) or TR$^-$ rats (Suzuki and Sugiyama, 1998; Konig et al., 1999).

Recently, it has been found that some organic anions can also be substrates of other ABC transporters. Multidrug resistance 1 (MDR1/ABCB1) preferentially accepts hydrophobic cationic or neutral compounds (Tanigawara, 2000; Varadi et al., 2002). However, Cvetkovic et al. (1999) reported that fexofenadine, an anionic nonsedating antihistamine, could be transported by human MDR1 (Cvetkovic et al., 1999). It has also been reported that estradiol-17β-D-glucuronide (EG) is a substrate of MDR1 as well as MRP2 in humans (Huang et al., 1998). Regarding the sulfated conjugates, we previously found that the biliary excretion clearance of the sulfates of 6-hydroxy-5,7-dimethyl-2-methylamino-4-(3-pyridylmethyl) benzothiazole (E3040) and liquiritigenin were excreted into bile in EHBR to the same extent as in Sprague-Dawley rats (Shimamura et al., 1994; Takenaka et al., 1995), suggesting that biliary excretion of sulfate conjugates is not mainly mediated by Mrp2 in rats. Suzuki et al. (2003) demonstrated that breast cancer resistance protein (BCRP/ABCG2) accepts various kinds of organic anions and preferentially transports sulfate conjugates (Suzuki et al., 2003). Taking into consideration the finding that MDR1 and BCRP are expressed in the canalicular membrane (Thiebaut et al., 1987; Maliepaard et al., 2001) in addition to these other facts, not only MRP2 but also MDR1 and BCRP can be involved in the biliary excretion of organic anions.

The double-transfected Madin-Darby canine kidney II (MDCKII) cell lines expressing both organic anion-transporting polypeptide 1B1 (OATP1B1/OATP-C/OATP2) or OATP1B3 (OATP8) in the basolateral membrane and MRP2 in the apical membrane, have been established as an in vitro model of hepatic vectorial transport of organic anions in humans (Cui et al., 2001; Sasaki et al., 2002). In this system, we can observe clear vectorial transport of bisubstrates for uptake and efflux transporters from the basal to the apical side compared with that in the opposite direction. The advantage of this double transfectant system is that it is able to evaluate the transport activities of apical transporters more sensitively compared with membrane vesicles. For example, with pravastatin (PRA), an anionic HMG-CoA reductase inhibitor, the ATP-dependent uptake is very small in human canalicular membrane vesicles (Niinuma et al., 1999), whereas the transcellular transport activity of PRA in OATP1B1/MRP2 double transfectant is large enough to observe its saturation kinetics (Sasaki et al., 2002).

In the present study, we constructed new double transfectants, expressing OATP1B1/MDR1 and OATP1B1/BCRP, and investigated the transcellular transport of organic anions to determine which transporters are involved in the biliary excretion. OATP1B1 is exclusively expressed in human liver and accepts many kinds of organic anions (Abe et al., 1999; Hsiang et al., 1999; Konig et al., 2000), and very recently, Hirano et al. (2004) showed that pitavastatin and EG are mainly taken up by OATP1B1 across the human basolateral membrane (Hirano et al., 2004). Accordingly, ligands can efficiently reach the efflux transporters from the intracellular compartment via OATP1B1, which makes this system useful for the characterization of the efflux transport of organic anions on the bile canalicular membranes. We investigated the transcellular transport of the following organic anions, EG and estrone-3-sulfate (ES), and HMG-CoA reductase inhibitors cerivastatin (CER) and PRA, to examine whether these compounds exhibited vectorial basal-to-apical transport in each double transfectant or not.

Materials and Methods

Materials. [^{3}H]EG (1.6 TBq/mmol) and [^{3}H]ES (2.2 TBq/mmol) were purchased from PerkinElmer Life and Analytical Sciences (Boston, MA). [^{3}H]CER (0.18 TBq/mmol) was synthesized by Hartmann Analytic GmbH (Braunschweig, Germany). [^{3}H]PRA (1.6 TBq/mmol) was kindly donated by Sankyo Co. Ltd. (Tokyo, Japan). Unlabeled CER was kindly donated by Bayer AG (Wuppertal, Germany). pEB6CAGMCS/SRZeo was kindly donated by Dr. Miwa (Tsukuba University, Tsukuba, Japan) (Tanaka et al., 1999). Parental MDCKII cells and MDCKII cells expressing human MRP2 (Evers et al., 1998) and MDR1 were kindly provided by Dr. Piet Borst (The Netherlands Cancer Institute, Amsterdam, The Netherlands). All other chemicals were commercially available and of reagent grade.

Construction of Plasmid Vector. Previously cloned human OATP1B1 cDNA in pcDNA3.1/Zeo (+) vector (Iwai et al., 2004) was subcloned into the NotI and XhoI sites of pEB6CAGMCS/SRZeo vector, which is an Epstein-Barr virus-based vector, and the subcloned gene was localized and replicated in the episome and not integrated into the genome of the host cells (Tanaka et al., 1999).

Cell Culture and Transfection of Expression Vector. Parental MDCKII cells and MDCKII cells expressing human MRP2 or MDR1 were cultured in Dulbecco's modified Eagle's medium (low glucose version) (Invitrogen, Carlsbad, CA) with 10% fetal bovine serum (Sigma-Aldrich, St. Louis, MO) and 1% antibiotic-antimycotic solution (Sigma-Aldrich) at 37°C under 5% CO_2. The transporter cDNA in the episomal expression vector was transfected into MDCKII cells using FuGENE6 reagent (Roche Diagnostics Co., Indianapolis, IN). At 50% confluence, cells on six-well plates were exposed to serum-free Dulbecco's modified Eagle's medium containing plasmid and FuGENE6 according to the manufacturer's instruction. At 6 h after the initiation of transfection, the plasmid-FuGENE6 solution was replaced with the normal culture medium. The transfected MDCKII cells were selected with Zeocin (700 μg/ml; Invitrogen).

Construction of Human BCRP-Expressing Cells. For constructing MDCKII cells expressing human BCRP, MDCKII cells were infected with recombinant adenoviruses containing human BCRP cDNA (Kondo et al., 2004) at 200 multiplicity of infection, 48 h prior to all experiments. The virus titer was determined as described previously (Kondo et al., 2004).

Western Blot Analysis. For Western blot analysis, crude membrane was prepared from MDCKII cells according to the method of the previous report (Gant et al., 1991). After the crude membrane was suspended in PBS, it was frozen in liquid N_2 and stored at −80°C until used. The protein concentrations in the crude membrane vesicles prepared from MDCKII cells were determined by the method of Lowry with bovine serum albumin as a standard. The membrane fraction was dissolved in 3× SDS sample buffer (New England Biolabs, Beverly, MA) with β-mercaptoethanol and loaded onto a 7% SDS-polyacrylamide electrophoresis gel with a 4.4% stacking gel. The molecular weight was determined using a prestained protein marker (New England Biolabs). Proteins were transferred electrophoretically to a polyvinylidene difluoride membrane (Pall, East Hills, NY) using a blotter (Trans-blot; Bio-Rad, Hercules, CA) at 15 V for 1 h. The membrane was blocked with Tris-buffered saline with 0.05% Tween 20 (TTBS) and 5% skimmed milk overnight at 4°C. After washing with TTBS, the membrane was incubated at room temperature in TTBS with 1000-fold diluted anti-OATP1B1 polyclonal antibody (Alpha Diagnostic International Inc., San Antonio, TX) for 1 h, 125-fold diluted monoclonal antibody against MRP2 (M_2III-6; Alexis Biochemicals, Gruenberg, Germany) for 2 h, 100-fold

diluted monoclonal antibody against MDR1 (C219; Signet Laboratories, Inc., Dedham, MA) for 1 h, or 200-fold diluted monoclonal antibody against BCRP (BXP-21; Kamiya Biomedical Company, Seattle, WA) for 2 h. For the detection of each transporter, the membrane was placed in contact with 2500-fold diluted donkey anti-rabbit (OATP1B1) or anti-mouse IgG (MRP2, MDR1, and BCRP) conjugated with the horseradish peroxidase (Amersham Biosciences Inc., Piscataway, NJ) for 1 h in TTBS. The band was detected using an ECL Plus Western blotting starter kit (Amersham Biosciences Inc.), and its intensity was quantified in a luminescent image analyzer (LAS-3000 mini; Fuji Film Corp., Tokyo, Japan).

Immunocytochemical Staining. For immunocytochemical staining, transfectants were plated at a density of 5×10^5 cells in 12-well plates, 96 h prior to the experiments. Sodium butyrate (5 mM) was added to the culture medium 1 day before the experiments. After fixation with methanol at −20°C for 10 min and permeabilization in 1% Triton X-100 in PBS at room temperature for 10 min, cells were incubated for 1 h at room temperature with 50-fold diluted anti-OATP1B1 rabbit serum, which was raised in rabbits against the 21 amino acids at the carboxyl terminus of the deduced OATP1B1 sequence (ESLNKNKHFVPSAGADSETHC), 40-fold diluted monoclonal antibody against MRP2 (M_2III-6), 40-fold diluted monoclonal antibody against MDR1 (C219), or 40-fold diluted monoclonal antibody against BCRP (BXP-21). Then, cells were washed with PBS three times and incubated for 1 h at room temperature with 250-fold diluted goat anti-rabbit IgG Alexa 488 (Molecular Probes Inc., Eugene, OR) for OATP1B1 or 250-fold diluted goat anti-mouse IgG Alexa 568 (Molecular Probes Inc.) for MRP2, MDR1, and BCRP. Nuclei were stained with 250-fold diluted TO-PRO-3 iodide (Molecular Probes Inc.). The localization was visualized by confocal laser microscopy (Zeiss LSM-510; Carl Zeiss Inc., Thornwood, NY).

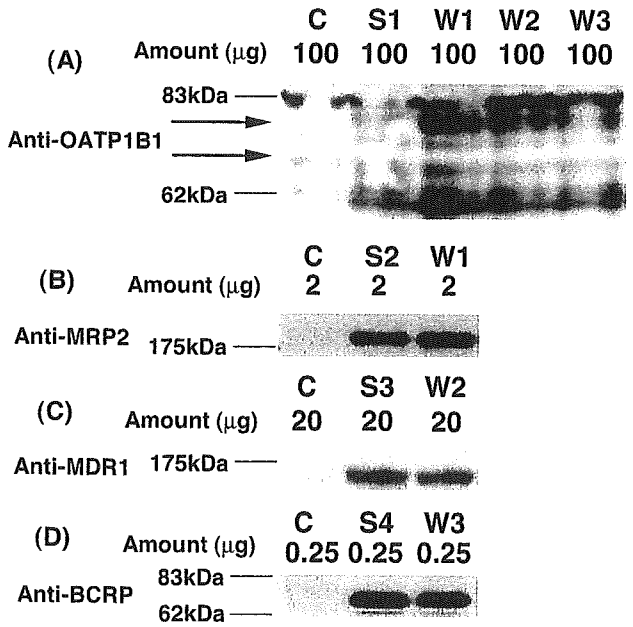

Fig. 1. Western blot analysis of OATP1B1, MRP2, MDR1, and BCRP in crude membrane vesicles obtained from MDCKII transfectants. Crude membrane prepared from MDCKII transfectants was separated by SDS-polyacrylamide gel electrophoresis. OATP1B1 was detected using polyclonal antibody against the carboxyl terminus of human OATP1B1 (A). MRP2, MDR1, and BCRP were detected using monoclonal antibody against the linker region of human MRP2 (B), MDR1 (C), and BCRP (D), respectively. The amount of protein applied to each lane in panel (A), (B), (C), and (D) was 100, 2, 20, and 0.25 μg. C, S1–4, W1–3 represent vector-transfected MDCKII cells, single-transfected cells (S1, OATP1B1; S2, MRP2; S3, MDR1; S4, BCRP), and double-transfected cells (W1, OATP1B1/MRP2; W2, OATP1B1/MDR1; W3, OATP1B1/BCRP). Arrows represent the specific bands for OATP1B1.

Transcellular Transport Study. The transcellular transport study was performed as reported previously (Sasaki et al., 2002). Briefly, MDCKII cells were grown on Transwell membrane inserts (6.5-mm diameter, 0.4-μm pore size; Corning Coster, Bodenheim, Germany) at confluence for 3 days, and the expression level of transporters was induced with 5 mM sodium butyrate for 24 h before the transport study. Cells were first washed with Krebs-Henseleit buffer (118 mM NaCl, 23.8 mM $NaHCO_3$, 4.83 mM KCl, 0.96 mM KH_2PO_4, 1.20 mM $MgSO_4$, 12.5 mM HEPES, 5.0 mM glucose, and 1.53 mM $CaCl_2$ adjusted to pH 7.4) at 37°C or 4°C. Subsequently, radiolabeled substrates were added in Krebs-Henseleit buffer either to the apical compartments (250 μl) or to the basolateral compartments (1 ml). After a designated period, the radioactivity in 100-μl medium in the opposite compartments was measured in a liquid scintillation counter (LS 6000SE; Beckman Coulter, Fullerton, CA). At the end of the experiments, the cells were washed three times with 1.5 ml of ice-cold Krebs-Henseleit buffer and solubilized in 500 μl of 0.2 M NaOH. After addition of 100 μl of 1 M HCl, 450-μl aliquots were transferred to the liquid scintillation counter for determination of radioactivity. Fifty-microliter aliquots of cell lysate were used to determine protein concentrations by the method of Lowry with bovine serum albumin as a standard.

Calculation of the Transport Activities of Recombinant MRP2, MDR1, and BCRP across the Double Transfectants. The apparent efflux clearance across the apical membrane ($PS_{apical,\ x°C}$) at each temperature (37°C or 4°C) was calculated by dividing the steady-state velocity for the transcellular transport ($V_{transcellular,\ x°C}$) of compounds determined over 2 h by the cellular concentration ($C_{cell,\ x°C}$) of the compounds determined at the end of the experiments (over 2 h) at each temperature (37°C or 4°C). The steady-state velocity for the transcellular transport was calculated by dividing the basal-to-apical transport amount at 2 h ($X_{x°C}$) when the steady-state condition was maintained (see *Results*) by 120 min. Then, to evaluate the activity of transporter-mediated transcellular transport, $PS_{apical,\ 4°C}$, the clearance at 4°C (at this temperature the active transport systems are not functional), was subtracted from $PS_{apical,\ 37°C}$. Moreover, since some endogenous efflux transporters have been reported to be expressed in MDCKII cells (Goh et al., 2002; Guo et al., 2002), the specific transport activity across the apical

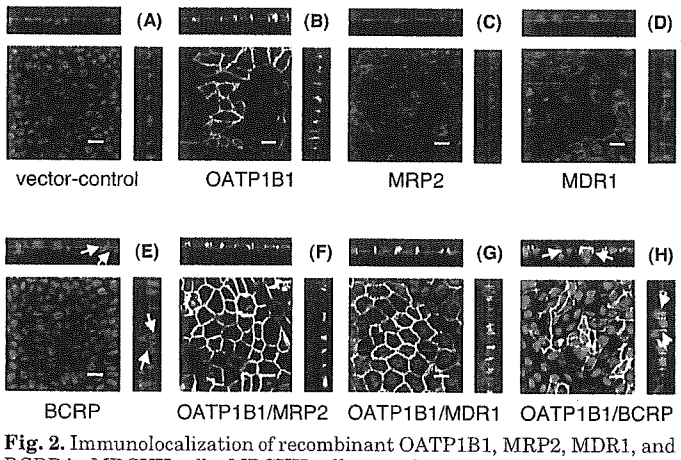

Fig. 2. Immunolocalization of recombinant OATP1B1, MRP2, MDR1, and BCRP in MDCKII cells. MDCKII cells transfected with empty vector (A), OATP1B1 (B), MRP2 (C), MDR1 (D), BCRP (E), both OATP1B1 and MRP2 (F), both OATP1B1 and MDR1 (G), and both OATP1B1 and BCRP (H) were stained with polyclonal antiserum against human OATP1B1 (green fluorescence, A–H), monoclonal antibody against human MRP2 (red fluorescence, A–C, and F), human MDR1 (red fluorescence, A, B, D, and G) and human BCRP (red fluorescence, A, B, E, and H). A and B show the staining with antiserum against human OATP1B1 and MDR1. The results were similar to the staining with antiserum against human OATP1B1/MRP2 or OATP1B1/BCRP (data not shown). Nuclei were stained with TO-PRO-3 (blue fluorescence). Pictures are single optical sections (x,y) (center) with xz (top) and yz (right) projections, respectively. Bar = 20 μm.

membrane (TA) mediated by exogenously expressed efflux transporters was calculated by subtracting the transporter-mediated clearance in each double transfectant from that in the single transfectant expressing only OATP1B1, as described in the following equations:

$$PS_{apical,x°C} = \frac{V_{transcellular,x°C}}{C_{cell,x°C}} \quad (1)$$

$$TA = (PS_{apical,37°C,double} - PS_{apical,4°C,double}) - (PS_{apical,37°C,single} - PS_{apical,4°C,single}) \quad (2)$$

Results

Expression of Human OATP1B1, MRP2, MDR1, and BCRP in MDCKII Cells. The expression of OATP1B1, MRP2, MDR1, and BCRP in double transfectants was confirmed by Western blot analysis (Fig. 1). Two major bands, which appeared at 83 and 62 kDa, could be detected in all kinds of OATP1B1-transfected cells (Fig. 1A), as shown previously (Konig et al., 2000). We were able to clearly detect human MRP2, MDR1, and BCRP with apparent molecular masses of about 190, 170, and 70 kDa (Fig. 1, B–D). The band also reacted slightly with the C219 antibody in wild-type MDCKII cells (Fig. 1C).

Localization of Recombinant Human OATP1B1, MRP2, MDR1, and BCRP. The cellular localization of the recombinant transporters in each transfectant was confirmed by confocal laser scanning microscopy. OATP1B1 was localized in the basolateral membrane (Fig. 2, B and F–H), whereas MRP2 and MDR1 were localized in the apical membrane (Fig. 2, C, D, F, and G). BCRP was mainly detected in the apical membrane, but part of the BCRP was also detected in the basolateral membrane (Fig. 2, E and H).

Transcellular Transport of EG, ES, CER, and PRA across the MDCKII Cell Monolayer. Transcellular transport of conjugated steroids EG and ES across the MDCKII monolayer was determined. As shown in Fig. 3, F–H, the basal-to-apical transport of EG was approximately 17, 6.7, and 8.8 times higher than that in the opposite direction in OATP1B1/MRP2, OATP1B1/MDR1, and OATP1B1/BCRP double transfectants, respectively, whereas the basal-to-apical flux of EG across the OATP1B1-expressing MDCKII cells was approximately 2.3 times higher than that in the opposite direction (Fig. 3B). A symmetrical flux of EG was observed across the control and MRP2-, MDR1-, and BCRP-expressing MDCKII cells (Fig. 3, A and C–E). For ES, the basal-to-apical transport was approximately 2.2-, 3.0-, 10-, and 41-fold higher than that in the opposite direction in OATP1B1-, OATP1B1/MRP2-, OATP1B1/MDR1-, and OATP1B1/BCRP-expressing MDCKII cells, respectively (Fig. 4 B and F–H). On the other hand, a symmetrical flux of ES was observed across the control and MRP2-, MDR1-, and BCRP-expressing MDCKII cells (Fig. 4, A and C–E). Transcellular transport of two kinds of HMG-CoA reductase inhibitors, CER and PRA, was also determined in the MDCKII transfectants. As shown in

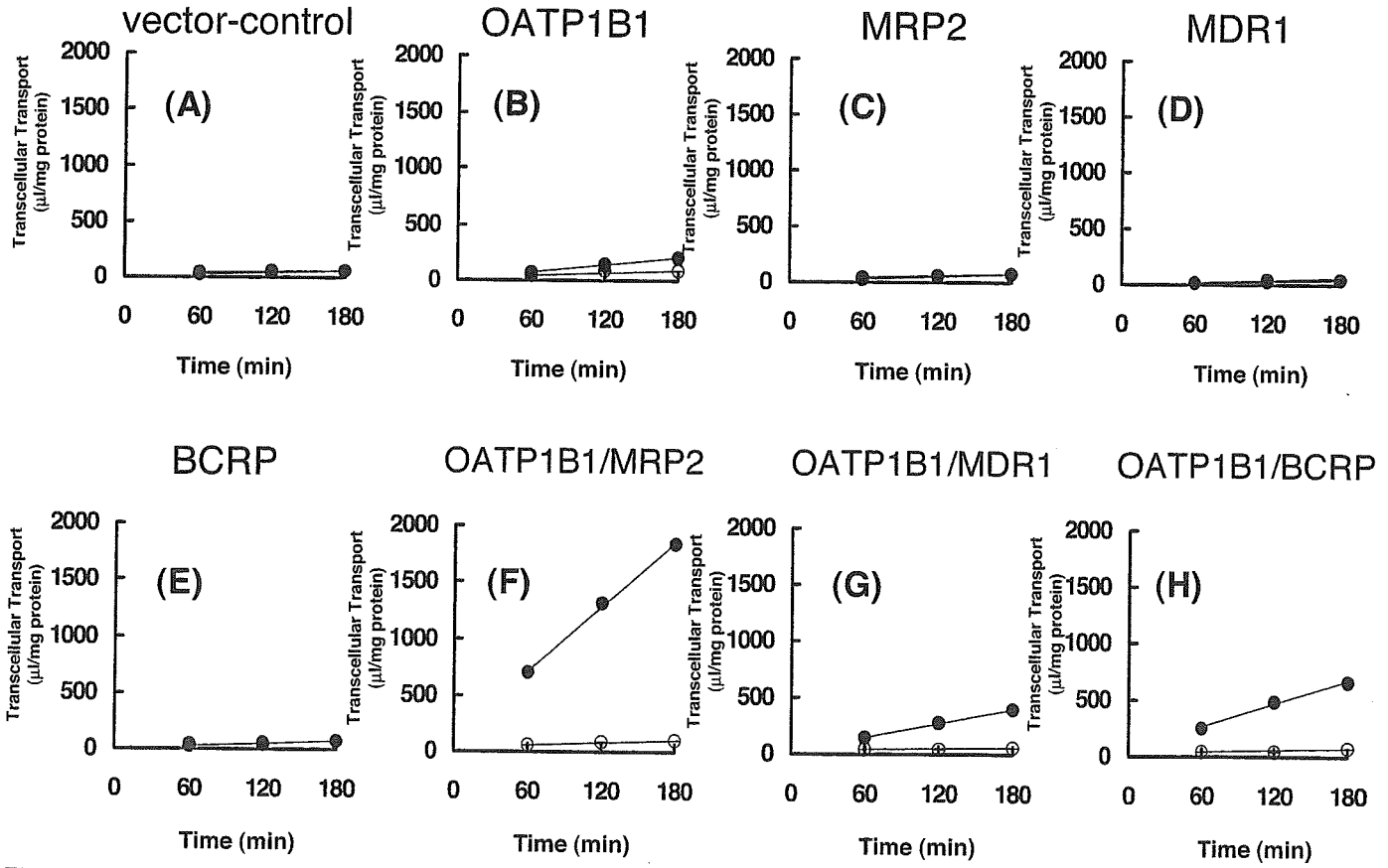

Fig. 3. Time profiles for the transcellular transport of [^{3}H]EG across MDCKII monolayers. Transcellular transport of [^{3}H]EG (0.5 μM) across MDCKII monolayers expressing OATP1B1 (B), MRP2 (C), MDR1 (D), BCRP (E), both OATP1B1 and MRP2 (F), both OATP1B1 and MDR1 (G), and both OATP1B1 and BCRP (H) was compared with that across the control MDCKII monolayer (A). Open and closed circles represent the transcellular transport in the apical-to-basal and basal-to-apical direction, respectively. Each point and vertical bar represents the mean ± S.E. of three determinations. Where vertical bars are not shown, the S.E. was contained within the limits of the symbol.

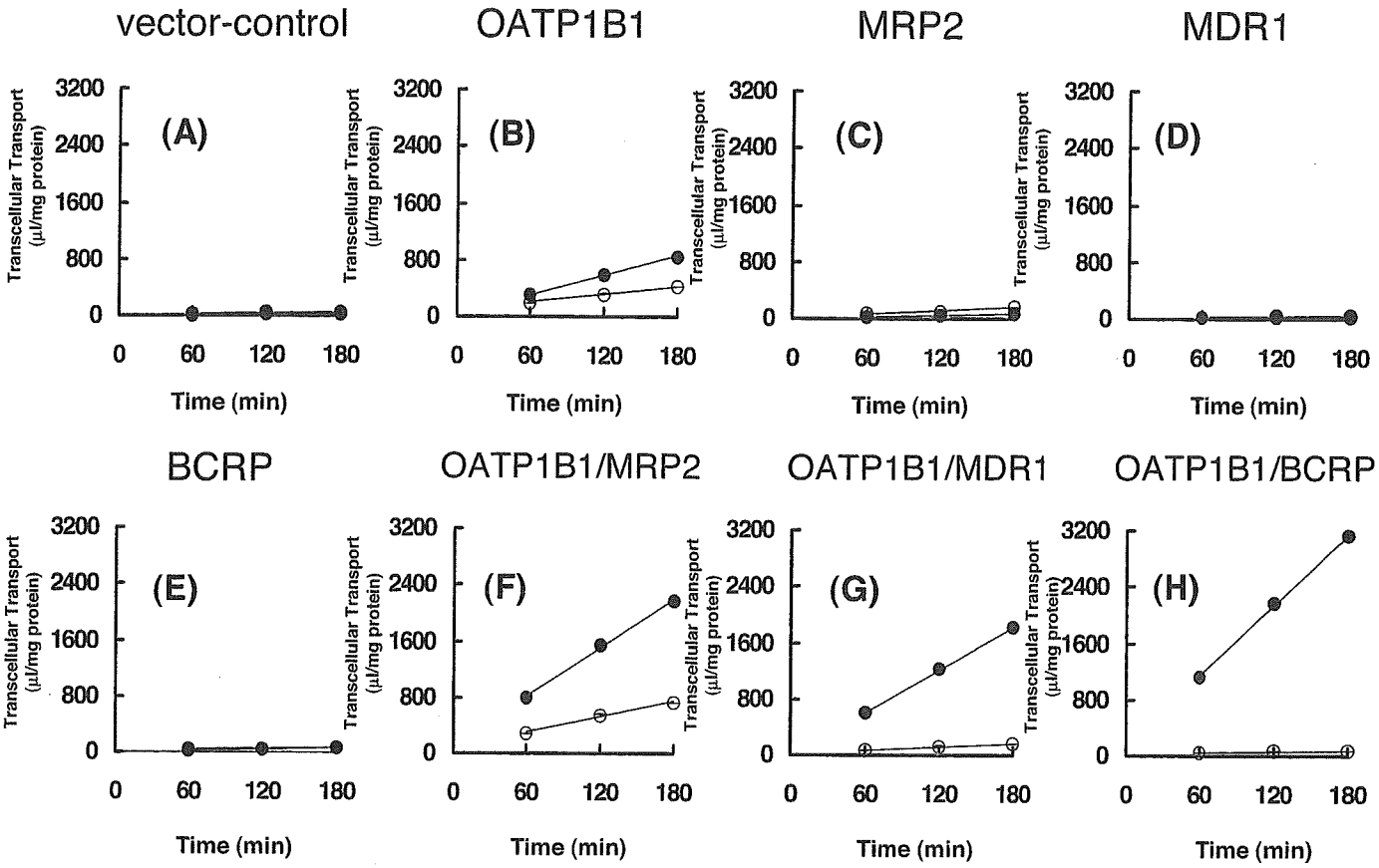

Fig. 4. Time profiles for the transcellular transport of [^{3}H]ES across MDCKII monolayers. Transcellular transport of [^{3}H]ES (0.5 μM) across MDCKII monolayers expressing OATP1B1 (B), MRP2 (C), MDR1 (D), BCRP (E), both OATP1B1 and MRP2 (F), both OATP1B1 and MDR1 (G), and both OATP1B1 and BCRP (H) was compared with that across the control MDCKII monolayer (A). Open and closed circles represent the transcellular transport in the apical-to-basal and basal-to-apical direction, respectively. Each point and vertical bar represents the mean ± S.E. of three determinations. Where vertical bars are not shown, the S.E. was contained within the limits of the symbol.

Fig. 5, F–H, the basal-to-apical transport of CER was 3.8, 6.3, and 3.1 times higher than that in the opposite direction in OATP1B1/MRP2-, OATP1B1/MDR1-, and OATP1B1/BCRP-expressing MDCKII cells, respectively, whereas a symmetrical flux of CER was observed across the control and all of the single transfectants (Fig. 5, A–E). On the other hand, the basal-to-apical flux of PRA was significantly 3.3-fold higher than that in the opposite direction only in OATP1B1/MRP2-expressing MDCKII cells (Fig. 6F). However, in the other cell lines, the ratio of the basal-to-apical flux to that in the opposite direction was less than two (Fig. 6, A–E, G, and H).

Calculation of the Transport Activities of Recombinant MRP2, MDR1, and BCRP across the Apical Membrane of the Double Transfectants. To estimate quantitatively the transport activity by the recombinant transporters across the apical membrane, the clearance to the apical compartment from cells (TA) was determined as described under *Materials and Methods*. The clearance for EG was 3.56 ± 0.07, 0.420 ± 0.026, and 0.383 ± 0.059 in OATP1B1/MRP2-, OATP1B1/MDR1-, and OATP1B1/BCRP-expressing MDCKII cells, respectively (Fig. 7A). The clearance for ES was 0.268 ± 0.013, 0.351 ± 0.011, and 2.31 ± 0.02 μl/min/mg protein in OATP1B1/MRP2-, OATP1B1/MDR1-, and OATP1B1/BCRP-expressing MDCKII cells, respectively (Fig. 7B). Regarding the statins, the clearance for CER was 0.612 ± 0.039, 0.669 ± 0.062, and 0.201 ± 0.007 μl/min/mg protein in OATP1B1/MRP2-, OATP1B1/MDR1-, and OATP1B1/BCRP-expressing MDCKII cells, respectively (Fig. 7C), whereas the clearance for PRA was 3.75 ± 0.112, 0.393 ± 0.097, and 0.194 ± 0.087 μl/min/mg protein, respectively (Fig. 7D).

Discussion

In the present study, we constructed new double transfectants expressing OATP1B1/MDR1 and OATP1B1/BCRP and observed the transcellular transport of four organic anions, EG and ES (steroid conjugates) and CER and PRA (HMG-CoA reductase inhibitors), to examine the substrate specificities and relative transport activities of the efflux transporters MDR1, MRP2, and BCRP. Western blot and immunocytochemical analyses revealed that OATP1B1, MRP2, and MDR1 were expressed in MDCKII cells and localized correctly on the basolateral (OATP1B1) and apical membranes (MRP2 and MDR1), respectively, but BCRP was localized mainly on the apical membrane and only partially on the basolateral membrane (Fig. 2). On the other hand, we could clearly observe significant basal-to-apical vectorial transport of organic anions in OATP1B1/BCRP double-transfected cells (Figs. 3–5), suggesting that minor expression of BCRP on the basal side does not affect the observation of the vectorial transport of substrates with our double transfectant, although basal-to-apical transport was thought to be partly inhibited by the basal expression of BCRP.